Effects of short flexible seagrass *Zostera noltei* on flow, erosion and deposition processes determined using flume experiments

Ganthy Florian [1, 2, 3, *], Soissons Laura [2], Sauriau Pierre-Guy [4], Verney Romaric [1], Sottolichio Aldo [2]

[1] IFREMER, Département Dynamique de l'Environnement Côtier, équipe PHYSED; BP 70 29280 Plouzané, France
[2] EPOC, CNRS; University of Bordeaux; allee Geoffroy St Hilaire, CS50023 33615 Pessac Cedex, France
[3] IFREMER, LER/AR; Quai du Commandant Silhouette 33120 Arcachon, France
[4] Littoral Environnement et Sociétés (LIENSs), CNRS; University of La Rochelle; 2 rue Olympe de Gouges 17000 La Rochelle, France

* Corresponding author : Florian Ganthy, email address : florian.ganthy@ifremer.fr

Abstract :

Innovative flume experiments were conducted in a recirculating straight flume. Zostera noltei meadows were sampled in their natural bed sediments in the field at contrasting stages of their seasonal growth. The aims of this study were: (i) to quantify the combined effects of leaf flexibility and development characteristics of Zostera noltei canopies on their interaction with hydrodynamics; and (ii) to quantify the role of Zostera noltei meadows in suspended sediment trapping and bed sediment resuspension related with changes in hydrodynamic forcing caused by the seasonal development of seagrasses. Velocity within the canopy was significantly damped. The attenuation in velocity ranged from 34 to 87% compared with bare sediments and was associated with a density threshold resulting from the flow-induced canopy reconfiguration. The reduction in flow was higher in dense canopies at higher velocities than in less dense canopies, in which the reduction in flow was greater at low velocities. These contrasted results can be explained by competition between a rough-wall boundary layer caused by the bed and a shear layer caused by the canopy. The velocity attenuation was associated with a two to three-fold increase in bottom shear stress compared with unvegetated sediment. Despite the increase in near-bed turbulence, protection of the sediment against erosion increased under a fully developed meadow, while sediment properties were found to be the main factor controlling erosion in a less developed meadow. Deposition fluxes were higher on the vegetated bed than on bare sediments, and these fluxes increased with leaf density. Fewer freshly deposited sediments were resuspended in vegetated beds, resulting in an increase in net sediment deposition with meadow growth. However, in the case of a very high leaf area index, sediment was mostly deposited on leaves, which facilitated subsequent resuspension and resulted in less efficient sediment trapping than in the less developed meadow.

Introduction

Intertidal mudflats are found worldwide and are major components of coastal ecosystem functioning. In response to hydrodynamic forcing or sediment availability, high rates of accretion or erosion can occur (up to several centimetres per tide, Deloffre et al., 2007) and hence modify the nature of bed

sediments, both in terms of grain size distribution and sediment concentration. Intertidal areas also support diversified biological populations, which can then interact with and alter erosion/deposition processes. Seagrasses constitute a highly productive compartment of coastal ecosystems and are known as ecosystem engineers (Madsen et al., 2001). Previous studies reported that seagrass beds dampen the hydrodynamic energy from tidal currents (Fonseca and Fisher, 1986; Gambi et al., 1990; Hendriks et al., 2008; Widdows et al., 2008) and waves (Koch, 1999; Koch and Gust, 1999; Madsen et al., 2001; Paul and Amos, 2011). Seagrass canopies are thus a low-energy environment which promotes sediment deposition (Gacia et al., 1999; Gacia and Duarte, 2001; Gacia et al., 2003; Hendriks et al., 2008; Ganthy et al., 2013) and reduces sediment resuspension (Ward et al., 1984; Gacia and Duarte, 2001; Amos et al., 2004; Bos et al., 2007; Widdows et al., 2008). This ecosystem engineering therefore tends to create stable habitats (Madsen et al., 2001).

Seagrass meadows are composed of a wide variety of species. Most investigations have focused on modifications in hydrodynamics and sediment dynamics by long-leaf seagrass beds, including *Posidonia oceanica* (Gacia and Duarte, 2001; Granata et al., 2001; Hendriks et al., 2008), *Zostera marina* (Fonseca and Fisher, 1986; Gambi et al., 1990; Fonseca and Koehl, 2006), *Syringodium filiforme* (Fonseca and Fisher, 1986), *Ruppia maritima* (Ward et al., 1984) or *Thalassia testudinum* (Fonseca and Fisher, 1986; Koch, 1999; Koch and Gust, 1999). All these studies highlighted specific species/water flow interactions, depending on the shape (Fonseca and Fisher, 1986), stiffness (Ghisalberti and Nepf, 2006; Peralta et al., 2008), density (Gambi et al., 1990; Peterson et al., 2004; van der Heide et al., 2007; Widdows et al., 2008), vertical distribution of biomass (Fonseca and Fisher, 1986; Bouma et al., 2005) and the fraction of the water column that they occupy (Ward et al., 1984; Bouma et al., 2005).

Resistance to flow is the most obvious hydrodynamic effect of submerged seagrasses leading to reduced current velocities within their canopy. This reduction in flow is usually accompanied by an increase in the flow above the canopy relative to the ambient flow due to its deflection over the canopy and loss of momentum within the canopy (Fonseca et al., 1983; Fonseca and Fisher, 1986; Gambi et al., 1990; Verduin and Backhaus, 2000; Peterson et al., 2004). This high-flow layer is usually called skimming flow. The lower part of the skimming flow is generally associated with a high turbulence region, while turbulence decreases near the bed, thereby affecting sediment erosion, deposition and vertical mixing (Nepf and Vivoni, 2000; Neumeier and Amos, 2004; Neumeier, 2007; Hendriks et al., 2008; Hendriks et al., 2010). These patterns are common to all types of vegetation. All the studies cited above recognized the major influence of vegetation features on plant/flow interactions. Hence, the change in vertical velocity and turbulence profiles will be qualitatively different if the vegetation is characterized by long or short, rigid or flexible, sparse or dense leaves.

When the vegetation is flexible, the drag force acting on vegetation stems and leaves will push them into more streamlined postures with increasing velocity. Compared with rigid vegetation, the canopy of flexible vegetation is subject to reconfiguration leading to significantly reduced drag (Koehl, 1984). De Langre (2008) proposed a simple model to qualitatively reproduce the canopy reconfiguration caused by the effects of wind on aerial canopies by balancing the opposing moments due to aerodynamic drag and plant stiffness. More recently, Luhar and Nepf (2011) proposed a model describing the flow-induced reconfiguration of buoyant, flexible seagrass blades through the balance between the posture-dependent drag and the restoring forces due to vegetation stiffness and buoyancy. The marked variability of vegetation-flow interactions implies a wide range of consequences for sediment transport processes (i.e. erosion, deposition). Aquatic meadows are often considered as net depositional areas where sediment resuspension is reduced and deposition is increased by the damping of hydrodynamic energy. By contrast, sediment scouring may occur on the edge of meadows or around individual shoots (Nepf, 1999; Chen et al., 2007; Hansen and Reidenbach, 2013). This transition from a depositional to an erosional environment may depend on the density of the vegetation which modifies the development of a skimming flow over the meadow: the diversion of horizontal flow around individual blades in low-density seagrass meadows is thought to induce scouring around individual shoots while vertical diversion above the meadow within a high-density seagrass canopy is thought to reduce water velocities and turbulence and promote sediment deposition (Lawson et al., 2012).

Zostera noltei is common in intertidal areas along the coasts of Europe and Africa. The species is relatively tolerant to hydrodynamics due to both its short plant stature (generally less than 20 cm in

height) and high flexibility. *Z. noltei* growth is characterised by a strong seasonal pattern, depending on its geographical location. For populations in the Arcachon lagoon (SW France), the main period of vegetative growth is March to September. Meadows degenerate from September to February but do not completely disappear from the sediment surface (Auby and Labourg, 1996) in contrast to populations in the Wadden Sea (van Katwijk et al., 2010). Compared with unvegetated areas, *Z. noltei* meadows in intertidal environments affect the morphodynamics of tidal flats over seasonal and long-term time scales (van Katwijk et al., 2010; Ganthy et al., 2013). The associated changes can be simulated and investigated using regional scale morphodynamic models. However, these models need to more accurately account for the effect of vegetation. Before using them, it is essential to identify a set of specific parameters (meadows/plant features) which modify both the mean flow and bed shear stress and hence sediment transport processes, and which can be included in model formulations. A further difficulty inherent to regional models is transferring small scale processes (at the scale of the canopy, i.e. < 1 m) to the scale of a model grid cell (i.e. several dozen metres).

Many flume studies have provided a detailed description of hydrodynamic processes within and around meadows, but very few investigated the erosion and deposition of fine sediments. Moreover, erosion experiments are a common way of determining critical thresholds of bed shear stress as a function of bed properties (Mitchener and Torfs, 1996; Amos et al., 2004; Ganthy et al., 2011, Jacobs et al., 2011). Most of these experiments used bare sediment, whereas erosion experiments using vegetated sediment are rarely reported in the literature (Widdows et al., 2008).

In the present study we investigated the interaction processes between *Z. noltei* meadows, current flows and cascading effects on erosion-deposition processes in specially designed recirculating flume experiments. The particular originality of this experimental protocol is the use of harvested blocks of bed sediment with its seagrass left in situ. Use of these sediment blocks ensures that the complex structure of natural seagrass meadows is captured in the flume.

This study advances knowledge on two novel topics:

1) The variability of plant-flow interactions at a seasonal time scale. We conducted a detailed investigation of the influence of *Z noltei* seasonal growth on changes in ambient flow and turbulence. This investigation is of primary importance as the seasonal variability of leaf length and density in *Z. noltei* meadows is probably unique in intertidal vegetated environments in Europe.

2) The changes in resuspension-deposition processes caused by *Z. noltei* meadows. We quantify for the first time the role of *Z. noltei* meadows in suspended sediment trapping and bed sediment resuspension compared with the effects of hydrodynamic alteration at a seasonal time scale.

MATERIALS AND METHODS

The changes in hydrodynamics, erosion and deposition processes caused by *Zostera noltei* canopies were measured under controlled conditions in the HYDROBIOS flume facilities at IFREMER l'Houmeau (see Orvain et al., 2003 for full details). Blocks of sediment with and without seagrasses were collected on a mudflat located in the central part of the Arcachon lagoon (Ganthy et al., 2011, 2013). At each sampling date, three stainless-steel rectangular box cores (0.4 m long × 0.3 m wide × 0.05 m thick) were pushed to a depth of 5 cm in the sediment, and base plates were placed below. The sampled boxes were then excavated from the surrounding sediment and immediately transported to the flume facility. The cores were placed in a holding container with sea water, light and air bubbling inputs. Holding for a period of 12 h allowed for the decrease in the abundance of bioturbators inside the meadows by their migration outside the vegetation toward the source of light. As the protocol used to transfer the samples from the tidal flat to the flume facilities was the same each time, we can safely assume disturbance was minimized and uniform in all tests.

After the holding period, the three cores were placed inside the flume, forming a 0.9 m long by 0.4 m wide test section. The narrow space between adjacent cores was filled with sediment from an additional core. This method, described by Widdows et al. (2008), created a continuous and almost undisturbed bed of natural sediment and seagrasses. The flume was then smoothly filled with fully aerated filtered seawater (1.3 m^3 for a water depth of 0.2 m) to protect the bed from disturbance. Salinity was adjusted to 30-31 at the beginning of the experiment and then measured regularly during the experiment, as along with temperature (Table 1).

Five experiments (T1 to T5) were performed between March and September 2010 (Table 1) to investigate the effects of seagrasses on hydrodynamics and sediment transport at different development stages of the plants. A control experiment (Tsed) was also performed on bare sediments. For this experiment, three box cores were sampled in an unvegetated area in the same tidal flat using the same protocol as for vegetated cores.

Each experiment consisted of three phases corresponding to three key sediment processes:

- P1 - initial bed erosion, investigated by increasing the flow rate (free stream velocity, U_∞, ranging from 0.1 m.s^{-1} to 0.4 m.s^{-1} in increments of 0.1 m.s^{-1} with each step lasting 90 minutes); the strategy used by many authors to investigate erosion fluxes, and when possible, to determine critical erosion shear stress and erosion rates (Amos et al., 2004, 2010; Ganthy et al., 2011; Jacobs et al., 2011).
- P2 - sediment deposition, investigated by seeding the flume with sediments and decreasing the flow rate (U_∞ ranging from 0.4 m.s^{-1} to 0 m.s^{-1} in increments of 0.1 m.s^{-1} with each step lasting 90 minutes); the objective was to investigate the dynamic response of suspended sediments, i.e. sediment trapping, to the presence of vegetation, and differences caused by the seasonal growth of the meadows, as previously investigated by Amos et al. (2004) in the Venice lagoon.
- P3 - remobilization of the freshly deposited sediments, investigated by the increasing flow rate (similar to phase P1, but with each step lasting only 45 minutes). Contrary to P1, the sediments were not consolidated, and the objective was to investigate conditions for net deposition after a tidal cycle related to sediment accumulation.

During the night between each experimental phase, the flow was stopped to allow the eroded sediments to settle. Note that the free stream velocity, U_∞, denotes the depth averaged velocity upstream from the seagrass bed or bare sediment bed.

Table 1. Main settings of experiments: sampling date, averaged water temperature and salinity along experiments and their associated standard deviations.

Test	T1	T2	T3	T4	T5	Tsed
Sampling Date	16-Mar	30-Mar	13-Apr	27-Apr	06-Sep	30-Mar
T (°C)	14.9 ± 0.5	17.0 ± 0.4	16.8 ± 0.3	19.7 ± 0.5	22.3 ± 0.1	17.1 ± 0.5
S_l (‰)	29.9 ± 0.1	30.6 ± 0.1	31.3 ± 0.2	31.4 ± 0.1	29.6 ± 0.2	31.0 ± 0.1

Hydrodynamic properties within the canopy

ADV measurements
Flow was measured using a Nortek$^©$ Acoustic Doppler Velocimeter (ADV, Vectrino) mounted on a 3D positioning system (ISEL$^©$), where x was carefully defined as the position along the flume channel axis, y as the distance across the flume and z as the vertical dimension. For each velocity step during the first phase of the experiments, four velocity profiles were performed. The first x-position of the vertical profile was located as far from the upstream edge of the meadow as possible (-0.15 m, Fig. 1), while the three other profiles were performed respectively at +0.15, +0.45 and 0.75 m downstream from the leading edge of the vegetation. During the second (P2) and third phase (P3), two velocity profiles were performed at -0.15 m and +0.45 m from the leading edge of the vegetation. The vertical ADV measurement positions started close to the bed ($z = 0.003$ m) up to the highest possible altitude where the ADV probe was fully submerged ($z = 0.143$ m). The step size was set at 0.003 m near the bed (from 0.003 to 0.047 m) and at 0.008 m in the upper part of the profile (from 0.047 to 0.143 m). For each position in the vertical profile, the ADV sampling rate was set at 8 Hz over a period of 32 s. This choice was a compromise between 1) sufficient samples per burst to compute turbulence parameters, 2) enough vertical measurements points distributed to precisely quantify plant-flow interactions (zostera leaves range from a tenth of a centimetre to a few centimetres in length), 3) and technical sampling rate limitation (8 Hz). A literature search for protocols used to collect turbulent measurements in similar environments revealed that although one thousand samples is the optimal

choice, many studies have successfully measured turbulence with a sampling strategy similar to the one used here (Neumeier and Ciavola, 2004; Leonard and Croft, 2006; Hasegawa et al., 2008; Chen et al., 2011). Turbulence values and ranges measured in this study are fully comparable with all other studies dedicated to plant-flow interactions.

To obtain reliable ADV measurements within the canopies, seagrass leaves located directly under the ADV were cut for the vertical profiles inside the canopy so that the sampling volume of the ADV would not be disturbed by the leaves.
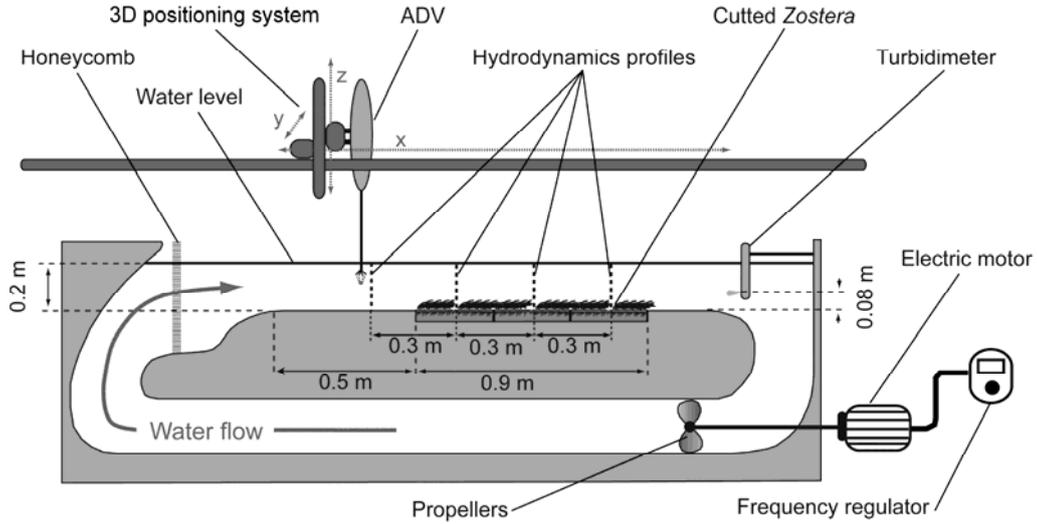

Fig. 1. Schematic view of the HYDROBIOS flume device.

An ADV device simultaneously records nine values per sample: three velocity components, three signal strength values, and three correlation values. Signal strength and correlation values were primarily used to determine the quality and the accuracy of the velocity data. A preliminary velocity signal check was performed prior to the computation of time-averaged velocity components and turbulence parameters. It consisted in removing all low signal-to-noise ratio data (<5 dB) and low correlation samples (<60%), according to Chanson et al. (2008). The Doppler spikes were then removed using the method described by Cea et al. (2007) based on minimum/maximum velocity thresholds expressed as:

$$u_{min} = U - \sqrt{2\ln(N)}\sigma_u \qquad (1a)$$

$$u_{max} = U + \sqrt{2\ln(N)}\sigma_u \qquad (1b)$$

where u_{min}/u_{max} are the minimum and maximum velocity thresholds in the x-direction, U is the time-averaged velocity in the x-direction, σ_u is the standard deviation of U, and N is the total number of data. Similar expressions are used for the other two velocity components. This despiking procedure was repeated iteratively until all data outside that range were removed.

Using this filtering process, the profiles recorded during the first experimental phase (P1) did not appear to be sufficiently reliable to compute turbulence properties (more than 50% of removed samples). A reflexion phenomenon was suspected and attributed to the lack of suspended sediments. The time-averaged velocities recorded during this experimental phase, should thus be interpreted with caution. However, for experimental phase P2, the filtering process removed less than 1% of the samples, so the turbulences profiles presented in this paper are those recorded during the second phase (P2), but are only available for distances of -0.15 m and +0.45 m from the leading edge of the vegetation.

At each vertical measuring point, the time-averaged velocity components U, V and W (corresponding to velocities in the x, y and z directions, respectively) were computed. The turbulent kinetic energy (TKE, in $m^2.s^{-2}$) was then computed as follows:

$$TKE = \frac{1}{2} \times \left(\overline{u'^2} + \overline{v'^2} + \overline{w'^2} \right) \qquad (2)$$

where u', v' and w' are the fluctuating velocity components in the x, y and z directions, respectively.

To compare the effects of seagrass on near-bed velocities, an attenuation coefficient of the velocity inside the canopy (AV_{can}, in %) was computed as the depth-averaged velocity attenuation inside the canopy:

$$AV_{can} = \frac{1}{N} \sum_{1}^{Hc_m} \left[\frac{100(U_s(z) - U_v(z))}{U_s(z)} \right] \qquad (3)$$

where N is the number of data inside the canopy, Hc_m is the measured canopy height (see below), $U_s(z)$ is the velocity at height z above the bed in the control test (Tsed) and $U_v(z)$ is the velocity at height z above the bed in the vegetated test (T1, T2, T3, T4 or T5) concerned.

Calculation of bottom shear stress

Various methods are described in the literature for the calculation of bottom shear stress (τ_b) values from measured instantaneous current velocities. The turbulent kinetic energy (TKE) method can be used to estimate the bottom shear stress proportionally to the *TKE* (Eq. 2) as follows: $\tau_b = C1 \times \rho \times TKE$, while *C1* is a constant coefficient and ρ the water density. *C1* coefficient values ranging from 0.19 to 0.21 are commonly cited in the literature for near-bed measurements in atmospheric or tidal boundary layers (Stapleton and Huntley, 1995; Kim et al., 2000). The coefficient *C1* was calibrated for turbulent flows over bare bed, and does not necessarily hold for canopy flows, so that for different types of flows (i.e. complex flows) the *C1* coefficient may have different values.

The Reynolds stress (RE) method also deals with turbulence measurements (Kim et al., 2000; Biron et al., 2004). In a log layer, the value of bed shear stress can be assumed to be close to the Reynolds shear stress ($\tau_b \approx \rho < -u'w' >$, where $< >$ denotes the time average). For a fully turbulent flow with a large Reynolds number, $<-u'w'>$ effectively becomes equal to the square of the friction velocity $u*^2$, providing a direct estimation of the bottom shear stress (Kim et al., 2000).

Considering these two different methods and their limitations for the estimation of the bottom shear stress in presence of complex flow fields, the RE method appeared to us to be the most physical. The bottom shear stress was thus determined using the RE method from the velocity measurements obtained at the first point above the bed (at $z = 0.003$ m). A section of the discussion is dedicated to comparing RE and TKE methods.

Sediment properties, erosion, and deposition

Bed sediment properties

The surface sediment properties were determined before and after each experiment in the uppermost 5 mm. In the tidal flat at, the same times as the box cores were sampled, one sediment sample (in triplicate) was collected by skimming the surface sediment closest to the sampled cores with a spatula. After emptying the flume at the end of the experiment, one set of triplicates per core was sampled at the mid-width, for a total of 3 sets of triplicates. Pre-weighed pill-boxes, with a known volume of $V_t = 3.2$ cm^3, were used to collect samples for the determination of the dry density of the sediments (ρ_{dry}, in kg.m^{-3}). The dry density was computed as $\rho_{dry} = (M_{dry} - M_p) / V_t$, where M_{dry} is the mass of dried sediments (after drying for 20 days at 60 °C), M_p is the mass of an empty pill box and V_t is the volume of a pill box. Grain-size analyses were performed using a Malvern laser particle sizer, measuring a size range from 0.06 to 800 µm. To prevent obstruction of the Malvern device, the samples were previously sieved through a 1 mm mesh to remove fragments of shells and seagrasses. Sediment diameters of the 10th, 50th, and 90th percentiles were obtained directly from the output of the Malvern device, and mud content (C_{mud}, in %) was then determined as the sediment fraction below a 63 µm grain size. Water content (W$_\%$, in %) was determined as $W_\% = 100 \times (M_{fresh} - M_{dry}) / (M_{dry} - M_p)$, where M_{fresh} is the mass of the filled pill box before drying. Water content was defined as the ratio between the mass of water contained by the sample and the mass of dried sediments, water content can thus exceed 100%.

The same treatment was applied to the seeded sediments (see below) for both the grain size analysis and dry density measurement (one triplicate). The main sediment characteristics of each experiment and control are summarized in Table 2.

Table 2. Main characteristics of bed sediment before and after experiments, and of seeded sediments.

Test		T1	T2	T3	T4	T5	Tsed
Sediment Bed Before Experiment	ρ_{dry} (kg.m^{-3})	$1\,015 \pm 60$	906 ± 81	855 ± 36	700 ± 110	566 ± 103	$1\,030 \pm 85$
	D_{10} (μm)	9.3 ± 1.4	6.4 ± 0.2	6.2 ± 0.5	5.2 ± 0.7	4.6 ± 0.2	8.9 ± 1.9
	D_{50} (μm)	138.5 ± 5.7	98.0 ± 5.6	96.8 ± 14.2	58.9 ± 30.2	40.6 ± 7.7	122.8 ± 12.8
	D_{90} (μm)	231.6 ± 4.7	214.0 ± 5.4	222.4 ± 4.7	209.6 ± 9.6	203.9 ± 11.8	241.9 ± 3.9
	C_{mud} (%)	24.4 ± 4.8	38.2 ± 1.1	38.9 ± 11.0	50.5 ± 10.5	56.8 ± 4.9	28.8 ± 6.6
Sediment Bed After Experiment	ρ_{dry} (kg.m^{-3})	$1\,198 \pm 68$	$1\,032 \pm 71$	$1\,018 \pm 64$	881 ± 139	715 ± 118	1123 ± 93
	D_{10} (μm)	9.2 ± 3.0	7.8 ± 4.0	6.0 ± 0.6	5.0 ± 0.6	4.4 ± 0.4	8.7 ± 2.3
	D_{50} (μm)	127.4 ± 19.4	99.6 ± 21.2	89.9 ± 22.6	65.6 ± 27	47.4 ± 13.1	117 ± 34.9
	D_{90} (μm)	226.3 ± 7.8	220.3 ± 9.9	219.5 ± 8.9	210.6 ± 12.6	213.2 ± 15.4	238.1 ± 27.0
	C_{mud} (%)	26.3 ± 8.9	34.9 ± 8.9	40.6 ± 6.7	48.6 ± 8.6	53.8 ± 4.7	31.3 ± 14.9
Seeding Sediment	$Mseed_{fresh}$ (g)	9051.2	9014.7	9006.7	9004.9	9014.1	9018.12
	$Mseed_{dry}$ (g)	$5\,729.4 \pm 54.3$	$5\,706.3 \pm 54.1$	$4\,938.2 \pm 52.6$	$4\,937.4 \pm 52.2$	$5\,435.5 \pm 49.6$	$4\,944 \pm 52.1$
	ρ_{dry} (kg.m^{-3})	-	842 ± 4	835 ± 13	926 ± 9	930 ± 8	831 ± 7
	$SSC(t_0)$ (mg.l)	582.4	659.9	589.7	851.7	721.8	527.1
	D_{10} (μm)	-	7.3 ± 1.3	4.8 ± 2.0	4.9 ± 1.8	5.0 ± 1.4	6.2 ± 1.9
	D_{50} (μm)	-	96.5 ± 12.7	68.5 ± 18.9	73.7 ± 14.2	73.8 ± 9.0	78.6 ± 13.5
	D_{90} (μm)	-	228.8 ± 17.4	216.5 ± 23.1	224.8 ± 8.4	223.3 ± 13.8	229.8 ± 9.6
	C_{mud} (%)	-	36.2 ± 0.8	45.0 ± 1.2	42.1 ± 2.2	43.4 ± 2.6	46.1 ± 2.3

Table 3. Derived parameters from calibration curves of the turbidimeter associated with their correlation coefficient and probability, and maximum suspended sediment concentration reached after the flume was seeded (used for the normalization of SSC, in Fig. 8).

Test		T1	T2	T3	T4	T5	Tsed
Calibration of Suspended Sediment Concentration	a_{SSC} (-)	3.37	3.32	2.86	4.41	4.5	2.44
	b_{SSC} (-)	35.44	6.38	34.82	13.6	75.48	28.8
	R^2 (SSC) (-)	0.96	0.94	0.95	0.91	0.94	0.93
	p (SSC) (-)	<0.01	<0.01	<0.01	<0.01	<0.01	<0.01
	$SSC_{(t0)}$ (mg.L^{-1})	582.4	659.9	589.7	851.7	721.8	502.8

Concentration of suspended sediments, erosion and deposition fluxes

Turbidity was recorded (at 0.08 m above the bed) at 2 Hz, with a 10 s burst at one minute intervals, using an optical turbidimeter (NKE© STBD) located 0.15 m downstream from the end of the test section. Suspended sediment concentration (*SSC*, in mg.l^{-1}) was determined by calibration of the turbidity signal against triplicate water samples. Triplicate water samples were taken in the flume during the course of each experiment at each velocity step (12 triplicates per experiment), just before the velocity was changed. Samples were collected using a plastic pipe plunged into the flume close to the turbidimeter probe (at the same height above the bed, and 2 cm downstream from the turbidimeter probe). Samples were filtered onto pre-weighed glass-fiber filters (GFC), washed with distilled water, dried for 48 h at 60 °C and re-weighed. Linear calibration curves were produced as $SSC = a_{SSC} \times N + b_{SSC}$, where N is the turbidity and a_{SSC} and b_{SSC} are calibration coefficients (Table 3). Total *SSC* was then averaged over each burst (10 s burst).

For each experimental phase, the instantaneous eroded or deposited sediment mass $M_{e/d}(t)$ was computed as $M_{e/d}(t) = (SSC(t) - SSC(t-1)) \times V_f$, where V_f is the water volume of the entire flume (the flume and the recirculation pipe; equal to 1.3 m^3). The total $M_{e/d}(t)$ was then determined for each velocity step, and the erosion (*E*) or deposition (*D*) fluxes (E_{P1}, D_{P2} and E_{P3} for phases P1, P2 and P3, respectively) were computed by dividing this mass by the product of the active erosion/deposition surface area (*S*) with the duration of the step. For the first experimental phase (P1- initial bed sediment erosion), the erosion surface area was the surface of the test section ($S_{P1} = 0.36$ m^2), while the step lasted 90 min. For the second experimental phase (P2 - sediment deposition), the main uncertainty concerned the effective deposition area within the channel. This parameter was difficult to quantify, as it can be altered by turbulence within the channel. For that reason, we considered that deposition occurred over the total bed area of the flume ($S_{P2} = 2.4$ m^2) across the whole phase, and the step lasted 90 min. This choice would only influence the absolute deposition flux values, while the relative values of the results would remain unchanged. For the third experimental phase (P3 - erosion of freshly deposited sediment), the erosion was also considered to occur over the total area of the flume ($S_{P3} = S_{P2}$), but the step lasted only 45 min.

Only one turbidity probe was available for this study and turbidity was consequently measured at only one height above the bed within the flume. The implications of this are described in the discussion section.

Sediment trapping by canopies

At the beginning of the second experimental phase (P2), the flow velocity was first set to 0.4 m.s^{-1}. The flume was seeded with the natural sediments previously collected at the sampling site. Sediments were collected on the bare mud site located nearest to the seagrass sampled. Only the surface sediments were sampled (0-0.02 m) and sieved (<1 mm) to remove macrofauna, coarser particles and shell fragments. This sediment was then homogenized at regular intervals. Before seeding, a fresh mass of fluid sediment (approximately 9000 g of $Mseed_{fresh}$, Table 2) was prepared after homogenization. The effective dry sediment mass ($Mseed_{dry}$, in g) added into the flume was determined as $Mseed_{dry} = Mseed_{fresh} \times (100 + W_{\%})$, where $W_{\%}$ is the water content based on the sediment properties of the seeding sediment. The actual dry densities in the different experiments (T2, T3, T4, T5 and Tsed) differed slightly due to incomplete homogenization. However, because the grain size characteristics were similar (except in test T2), only the effective mass of the dry sediment ($Mseed_{dry}$) was affected. The characteristics of the seeded sediment used in the first test (T1) were unknown (Table 2), and for that reason, results of the sediment deposition (phase P2) and subsequent erosion (phase P3) are not presented for this test. Once the flume was seeded, the free-stream velocity was maintained at its initial value ($U_\infty = 0.4$ m.s^{-1}) for 95 min to allow correct homogenization of the flume (5 min = 7 full volume recirculation cycles) and the duration of the first velocity step (90 min). Then, the free-stream velocity was decreased by increments of 0.1 m.s^{-1}, each step lasting for 90 min until a free stream velocity of 0.1 m.s^{-1} was reached. The flow was stopped at the end of the last velocity step.

Vegetation characteristics

During the first phase (P1) of each experiment on vegetated sediment (T1 to T5) and at each velocity step, the canopy height (Hc_m, in mm) was estimated by digital photography analysis, using a protocol adapted from Neumeier (2005). A frame of graph paper (0.3 m length × 0.21 m height) was placed on one side of the flume, with the base of the frame matching the bed sediment and the upstream and downstream sides of the frame matching the second core (x = 0.3 to 0.6 m). Digital photographs were always taken at exactly the same location and distance from the side of the flume to ensure that the sides of the photograph coincided with the graph paper frame. The canopy height (Hc_m) was estimated as the height of the top of canopy, averaged over the width of the photograph.

After each experiment, vegetation characteristics were determined following the French protocol for estimating the ecological status of *Z. noltei* beds under the European Water Framework Directive (Auby et al., 2010). One mini-core (98 mm in diameter and the total thickness of bed sediment – 50 mm) was sampled per box core (one triplicate per test). Samples were washed with fresh water on a sieve with a mesh size of 1 mm, to separate the seagrasses from sediments and shell fragments. Seagrasses were then separated into individual plants, and the plants were divided into above- and below-ground biomass. The number of shoots per sample was recorded, providing the shoot density (D_{shoot}, in m^{-2}). The length and width of leaves were measured on ten randomly selected shoots, and used for the computation of the mean leaf length (L_{leaf}, in mm), mean leaf width (w_{leaf}, in mm), mean leaf area index (LAI, total leaf area per ground area, dimensionless). The leaf density (D_{leaf}, in m^{-2}) was computed as the product of shoot density and the mean number of leaves per shoot. The above-ground biomass (B_{above}, in g.m^{-2}) was calculated after the shoots were dried at 60 °C. The mean and standard deviation of each parameter were then computed for each experiment and are summarized in Table 4.

Table 4. Main vegetation characteristics associated with measured canopy heights depending on the free stream velocity.

	Test	T1	T2	T3	T4	T5
	B_{above} (g.m^{-2})	14.9 ± 5.3	21.4 ± 3.4	26.0 ± 8.9	60.6 ± 14.8	102.2 ± 37.1
	LAI (~)	0.85 ± 0.25	1.42 ± 0.17	1.78 ± 0.78	4.21 ± 1.70	9.03 ± 0.98
	L_{leaf} (mm)	56 ± 6	72 ± 7.8	76 ± 25.8	63 ± 13.5	150 ± 7.9
	w_{leaf} (mm)	0.56 ± 0.04	0.58 ± 0.03	0.63 ± 0.01	0.82 ± 0.05	1.21 ± 0.02
	D_{shoot} (×10^3 m^{-2})	7.96 ± 2.52	9.53 ± 0.87	8.22 ± 3.47	12.58 ± 1.85	18.23 ± 4.78
Biometry	D_{leaf} (×10^3 m^{-2})	26.65 ± 6.46	34.19 ± 1.31	42.54 ± 1.83	80.94 ± 2.21	51.08 ± 7.82
	Hcm (U=0.1) (mm)	35 ± 5	40 ± 7	37 ± 6	47 ± 8	93 ± 11
	Hcm (U=0.2) (mm)	25 ± 4	35 ± 5	24 ± 4	35 ± 5	73 ± 8
	Hcm (U=0.3) (mm)	20 ± 4	24 ± 4	22 ± 3	28 ± 3	59 ± 6
	Hcm (U=0.4) (mm)	15 ± 2	20 ± 3	16 ± 3	21 ± 2	48 ± 4

Statistical tests

Differences in sediment characteristics and *Zostera noltei* biometry between experiments were tested with one-way analyses of variance (ANOVA) with replication. The maximum type I error rate was set at 0.05. Homogeneity of variance was checked using Bartlett's test and if rejected, data were log10 transformed. Significant ANOVA results were followed by multiple comparisons using the conservative Tukey post-hoc test (Sokal and Rohlf, 1995). Correlations between variables were tested following critical values for the correlation coefficient (Rohlf and Sokal, 1981). Statistical analyses were performed with Minitab software 15.1.

To confirm the reliability of the parameterizations when relationships were found, the root mean squared error (RMSE) was also used:

$$RMSE = \sqrt{\frac{\sum_i^n (x_i - y_i)^2}{n}} \qquad (4)$$

where n is the number of value, x_i and y_i are the measured and predicted values, respectively, for the ith data value.
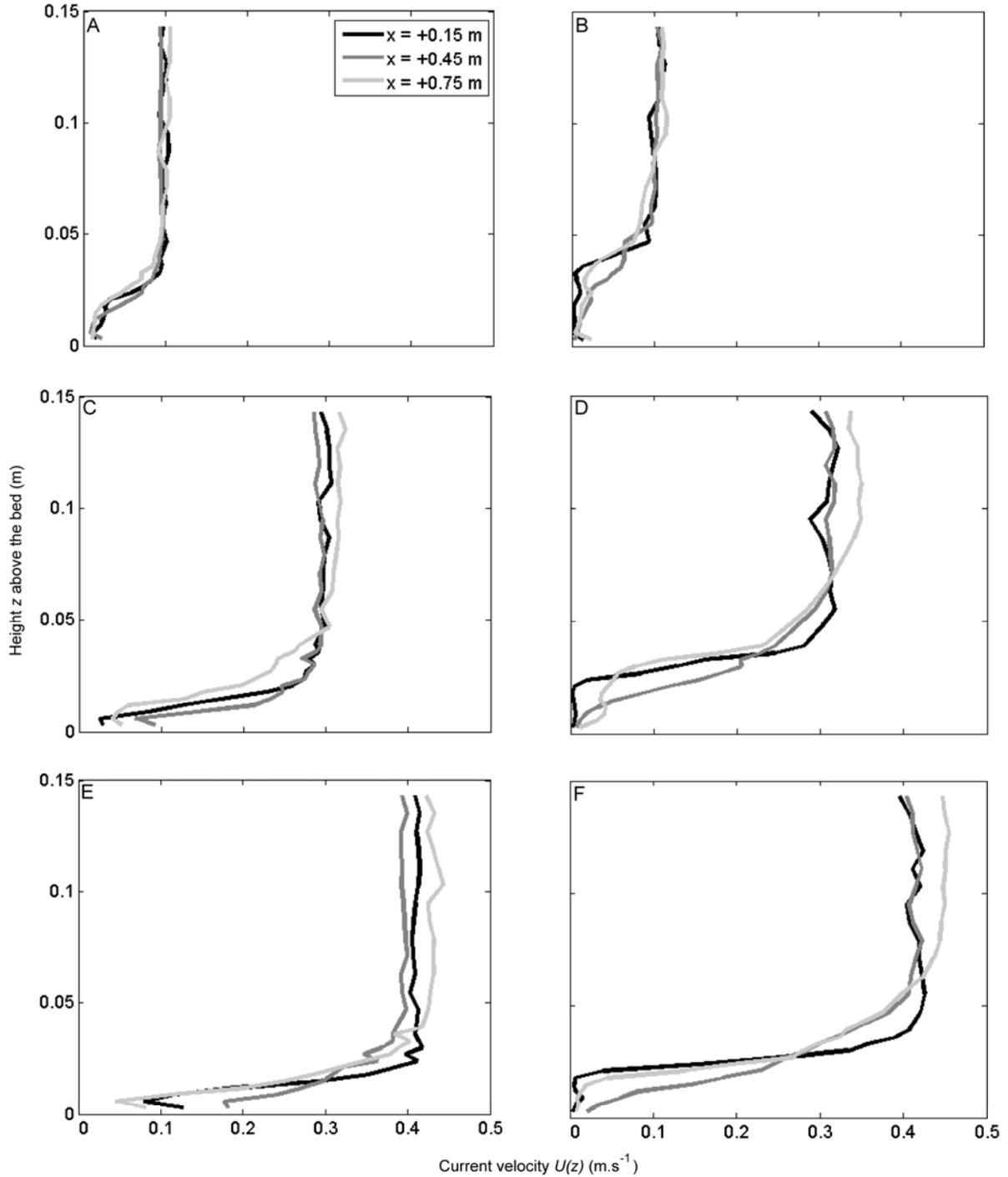

Fig. 2: Comparison of current velocity profiles recorded at 0.15, 0.45 and 0.75 m from the leading edge of the vegetation patch above different densities of *Zostera noltei*: A, C and E refer to the test T3 at free stream velocities of 0.1, 0.3 and 0.4 m.s-1 respectively, while B, D and F refer to the test T4 at free stream velocities of 0.1, 0.3 and 0.4 m.s-1 respectively.

RESULTS

Vegetation development

Both leaf area index (*LAI*) and above-ground biomass (B_{above}) significantly increased from test T1 to test T5 (p < 0.001). In the first three tests (T1 to T3), both B_{above} and *LAI* values were relatively low (14.9 – 26.0 g.m^{-2} and 0.85 – 1.78, respectively), denoting limited development of seagrass, while B_{above} and *LAI* values in tests T4 and T5 were significantly higher than in tests T1 to T3, with respectively 11-fold and 7-fold higher B_{above} and *LAI* values in T5 than in T1. Shoot density (D_{shoot}) values also increased significantly from test T1 to test T5 (p = 0.009), with 2.4-fold higher values in tests T4 and T5 than in T1. Leaf length (L_{leaf}) increased significantly from test T1 to T5 (p < 0.001) with maximum values in T5. Leaf density (D_{leaf}) also increased significantly from test T1 to T5 (p = 0.008 based on log10 values) but not continuously, denoting differences in the vertical distribution of plants between tests, as maximum values were recorded in test T4 (Table 4).
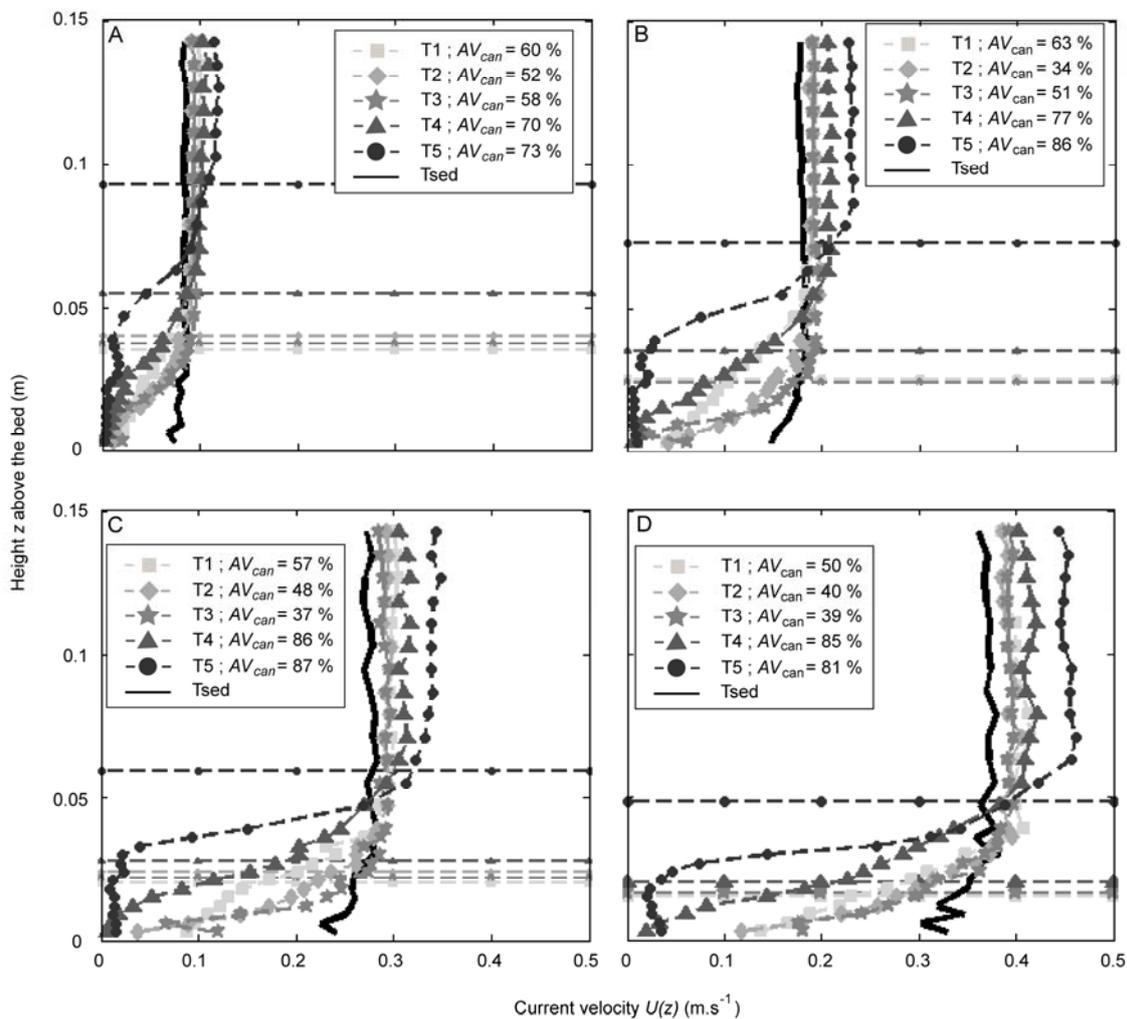

Fig. 3: Comparison of current velocity profiles recorded at 0.45m from the leading edge of the vegetation patch under free stream flow velocities of (A) 0.1 m.s^{-1}, (B) 0.2 m.s^{-1}, (C) 0.3 m.s^{-1} and (D) 0.4 m.s^{-1} above different densities of *Zostera noltei* (T1 to T5, dashed lines) and over bare sediments (Tsed as a control, solid black line). The measured canopy heights (Hc_m, horizontal lines) and the coefficient for velocity attenuation within the canopy (AV_{can}, eq. 3, in %) are presented.

Flow structure

A practical issue in flume studies is the distance required for the flow to fully develop. Profiles measured at three locations along the longitudinal test section were compared at different velocities and seagrass growth stages to validate the representativeness of the central profile that was subsequently used in all experimental phases (Fig. 2). Results showed that the flow developed rapidly during the experiments, and confirmed that observations made 45 cm downstream from the leading edge are fully reliable.

Vertical profiles of flow velocity ($U(z)$, m.s-1) measured above bare sediments (Tsed) compared to those measured over vegetated beds (T1 to T5, Fig. 3) demonstrated strong velocity damping near the bed for all of the vegetated beds. The velocity profile over bare sediments (Tsed) was characterized by an approximately constant velocity throughout most of the water column and only a slight decrease in velocity near the bed straight shape in its upper part, associated with a slight decrease in velocity near the bed. In contrast, all the velocity profiles obtained for the vegetated beds showed a more complex structure, which varied with seagrass densities and development (i.e., D_{leaf} and LAI, Table 4).

Velocity attenuation coefficients inside the canopy were the lowest in tests T1 to T3 (AV_{can} ranged from 34 to 63%), and these tests also had the lowest LAI values (0.85, 1.42 and 1.78, respectively in T1, T2 and T3). In tests T4 and T5 (LAI = 4.21 and 9.03, respectively), the velocity attenuation coefficient ranged from 75% to more than 85%.

Vertical profiles of the turbulent kinetic energy (TKE, Fig. 4) were characterized by a maximum value at approximately half the canopy height for the high-density vegetated beds (T4 and T5), while for the less-developed seagrass beds (T1 to T3) and the unvegetated bed (Tsed), the maximum value was measured close to the bed. Below this maximum, the TKE value decreased toward the bed although the TKE levels were generally significantly higher over vegetated beds than over bare sediment (Tsed). In contrast, above the maximum, the TKE values decreased upward until they reached a value lower than that of the control experiment (Tsed).

Bottom shear stress

Bottom shear stress values plotted against depth averaged velocities (Fig. 5) showed that bottom shear stress was generally significantly (up to 5-fold) higher in vegetated tests (T1 to T5) than in the unvegetated test (Tsed), except at low to moderate velocities in test T5, in which the seagrass was most developed (i.e. had the highest LAI). Values ranged from 0.036 to 0.261 N.m^{-2} at the lowest velocity in vegetated tests, and from 0.949 to 2.695 N.m^{-2} at the highest velocity. By contrast, values for the unvegetated bed (Tsed) ranged from 0.059 to 0.493 N.m^{-2}, respectively, for the lowest and the highest velocity.

Sediment characteristics, erosion and deposition

Sediment characteristics

Grain-size distributions of the initial bed sediments (Fig. 6A) were bimodal in all the tests, consisting in a narrow primary mode corresponding to fine sands (~0.2 mm) and in a wide secondary mode corresponding to fine silts (~0.01 mm). The relative ratio of the sediment fractions between these two modes varied significantly, depending on test concerned (i.e. sampling date). Test T1 showed the highest difference in fractions between the sandy and silty modes, while test T5 showed the smallest. Mud content (C_{mud}) of the bed sediments sampled in the field before the experiment (Table 2) revealed a 2.4-fold increase from test T1 (C_{mud} = 24.4 %) to T5 (C_{mud} = 56.8 %). This significant increase in mud content ($p < 0.001$) was associated with a significant decrease in dry density (ρ_{dry} ranging from 1015 to 700 kg.m^{-3} in T1 and T4, respectively).

Similar significant trends were also found in the bed sediments sampled after the end of each experiment ($p < 0.001$) with (C_{mud} = 26.3%, ρ_{dry} = 1198 kg.m^{-3}, D_{50} = 127.4 µm and C_{mud} = 53.8%, ρ_{dry} = 715 kg.m^{-3}, D_{50} = 47.4 µm in T1 and T5, respectively). Sediment characteristics of the test Tsed before and after the flume experiment were similar to those obtained in tests T1, T2 and T3, before and after the flume experiment ($p > 0.05$). Comparisons of sediment characteristics before and after

each flume experiment showed an increase in dry densities (p < 0.001), whereas no significant changes were found in mud contents (p = 0.83).

Grain-size distribution of seeded sediments (Fig. 6B) showed the same bimodal distribution in all the tests as that observed in the initial bed sediments, consisting in a narrow primary mode corresponding to fine sands (~0.2 mm) and in a wide secondary mode corresponding to fine silts (~0.01 mm).
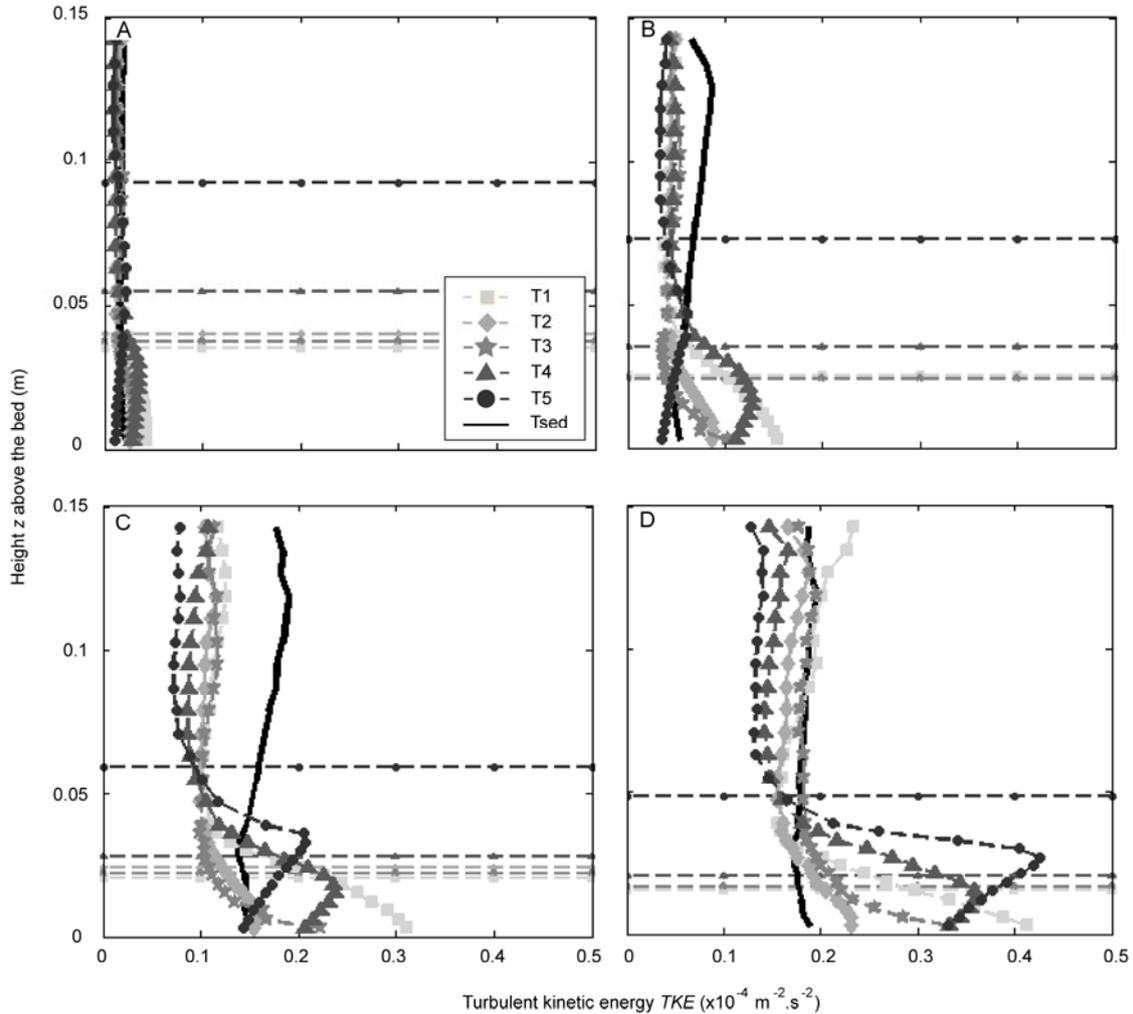

Fig. 4: Turbulent kinetic energy (*TKE*) profiles under free stream flow velocities of (A) 0.1 m.s^{-1}, (B) 0.2 m.s^{-1}, (C) 0.3 m.s^{-1} and (D) 0.4 m.s^{-1} above different densities of *Zostera noltei* (T1 to T5, dashed marked lines) and over bare sediments (Tsed as a control, solid black line). The measured canopy heights (Hc_m, horizontal dashed lines) are presented.

Erosion of initial bed sediments: Phase P1

A comparison of the *SSC* time series measured during the first experimental phase (P1) using vegetated beds (T1 to T5, Fig. 7A) with those with bare sediments (Tsed) revealed a similar step or stair shape for the free stream-velocity steps in all the tests. At lower velocities ($U_\infty = 0.1 - 0.2$ m.s^{-1}), the *SSC* tended to decrease slowly after reaching a maximum value at the end of the increase in velocity, while at higher velocities ($U_\infty = 0.3 - 0.4$ m.s^{-1}), the step or stair shape was more horizontal, with a plateau after a period of increase. Despite similar shapes among the curves, the *SSC* levels were different. The *SSC* obtained in tests T1, T2 and T5 (approximately 10 mg.l^{-1} at the end of the experiment) remained below the levels obtained in the control test using bare sediments (Tsed, approximately 15 mg. l^{-1} at the end of the experiment). The *SSC* in test T3 was generally similar to that in the control, while the *SSC* in test T4 was higher than that in the control test, with a value of 30 mg.l^{-1} at the end of the experiment.
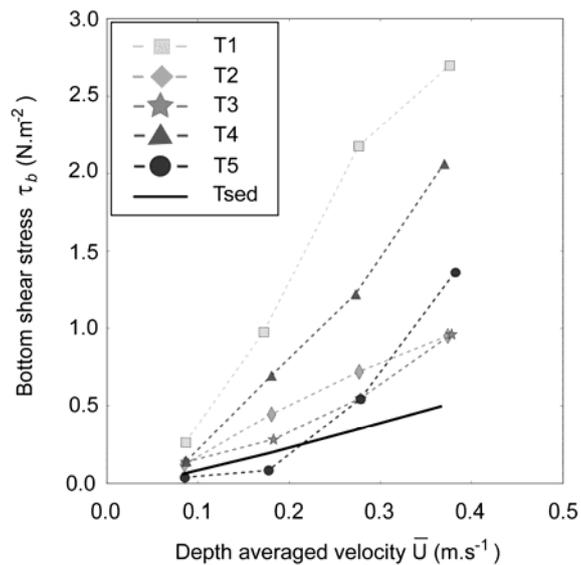
Fig. 5: The bottom shear stress (τ_b), computed using the RE method, as a function of the depth-averaged velocity ($\overline{U}$) for different densities of seagrass beds (T1 to T5, dashed marked lines) and control test over bare sediments (Tsed, solid black line).
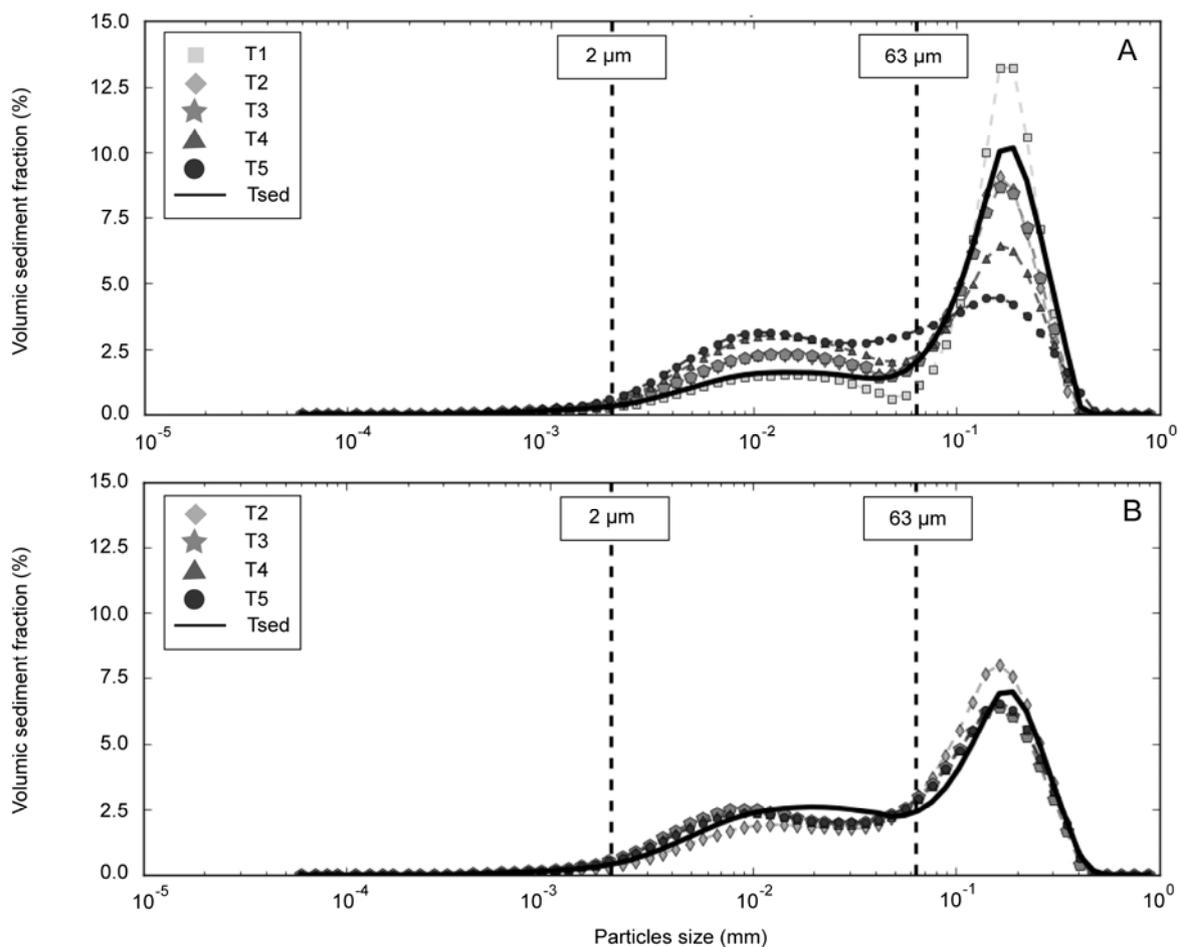

Fig. 6: Grain-size distribution (A) for surficial sediments before experiments and, (B) for seeded sediments. Size limits between granulometric clays and silts (2 µm) and between silts and sand (63 µm) are also indicated for a better readability.

Considering the relationship between erosion fluxes (E_{PI}) and bottom shear stress (τ_b) (Fig. 7B), all tests with vegetation had lower erosion fluxes than the control. Erosion fluxes in test T1 were the lowest ($E_{PI} < 5$ mg.m^{-2}.s^{-1}) despite the occurrence of the highest τ_b value during that test. Similar behaviours were observed in tests T2, T3 and T4, however with a very high flux at the highest free stream velocity ($E_{PI} = 13$ mg.m^{-2}.s^{-1} at $U_\infty = 0.4$ m.s^{-1}). While erosion fluxes in test T5,were similar to those in tests T2, T3 and T4, they tended to decrease with increasing free stream velocity.
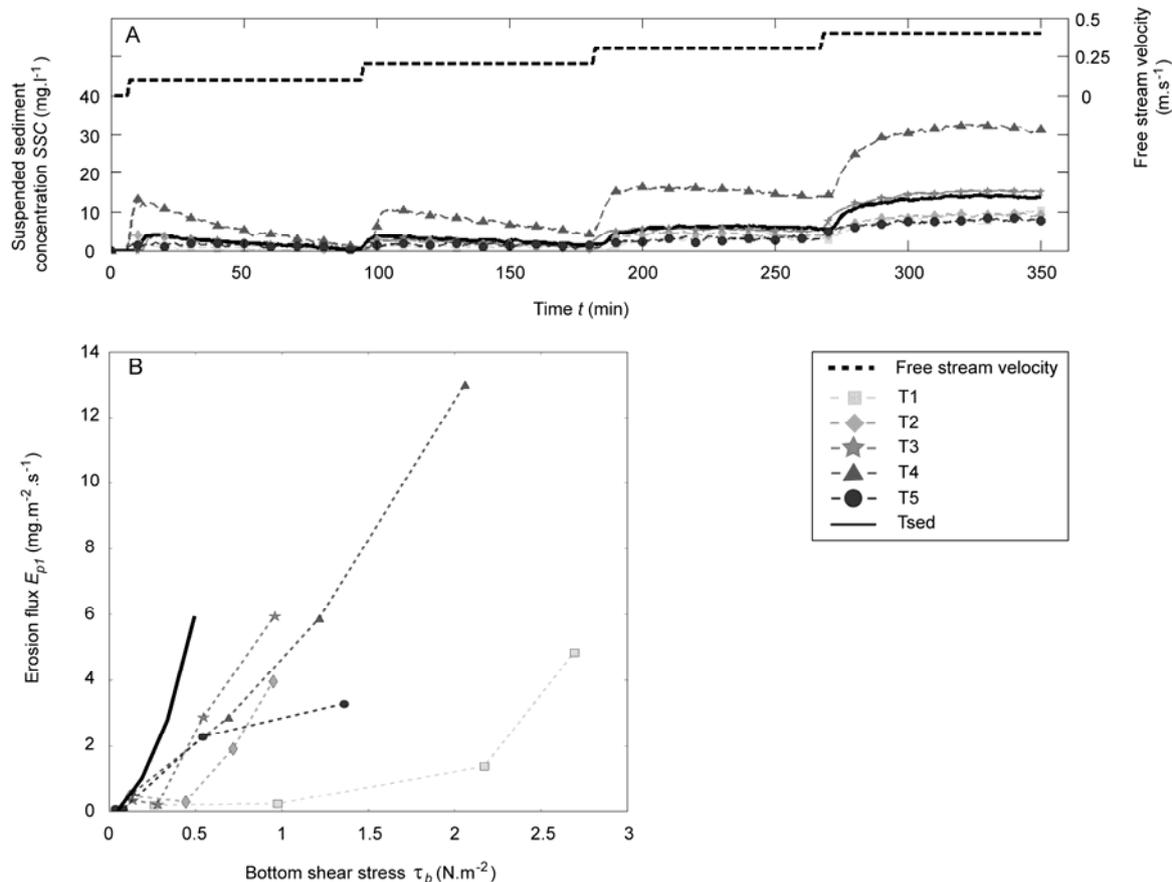

Fig. 7: (A) Time series of suspended sediment concentration during the first experimental phase (P1) over different densities of *Zostera noltei* (T1 to T5, dashed lines) and the control (Tsed, solid black line). Bold dashed black line corresponds to the free-stream velocity applied at each velocity step. (B) Relationship between erosion fluxes at each velocity step and bottom shear stress above vegetated beds (T1 to T5) and a bare sediment (Tsed).

Deposition of seeding sediments: Phase P2

As the characteristics of the seeded sediment in the first test (T1) were unknown (Table 2) results regarding sediment deposition are not presented for this test. However, in all the other tests, the particle deposition during the second experimental phase (P2, Fig. 8A) was significant and generally resulted in an exponential decrease in the normalized suspended sediment concentration ($SSC(t)/SSC(t_0)$). In the normalized concentrations, decay was higher in all the tests in the presence of vegetation (T2 to T5) than in the control test (Tsed). Tests with low seagrass densities (T2 and T3) showed the least decrease in normalized sediment concentrations, mainly when the free-stream velocity was high ($U_\infty = 0.4 - 0.3$ m.s^{-1}). However, tests T4 and T5 showed a marked decrease in normalized suspended sediment concentrations from $U_\infty = 0.3$ m.s^{-1} and at lower velocities. It is also notable that during the first velocity step ($U_\infty = 0.4$ m.s^{-1}) in the control test, the normalized sediment concentrations increased slowly, indicating absence of deposition but still significant erosion. We assume that flocculation processes were insignificant due to intense mixing caused by the presence of propellers associated with short recirculation times (40 to 160 s).
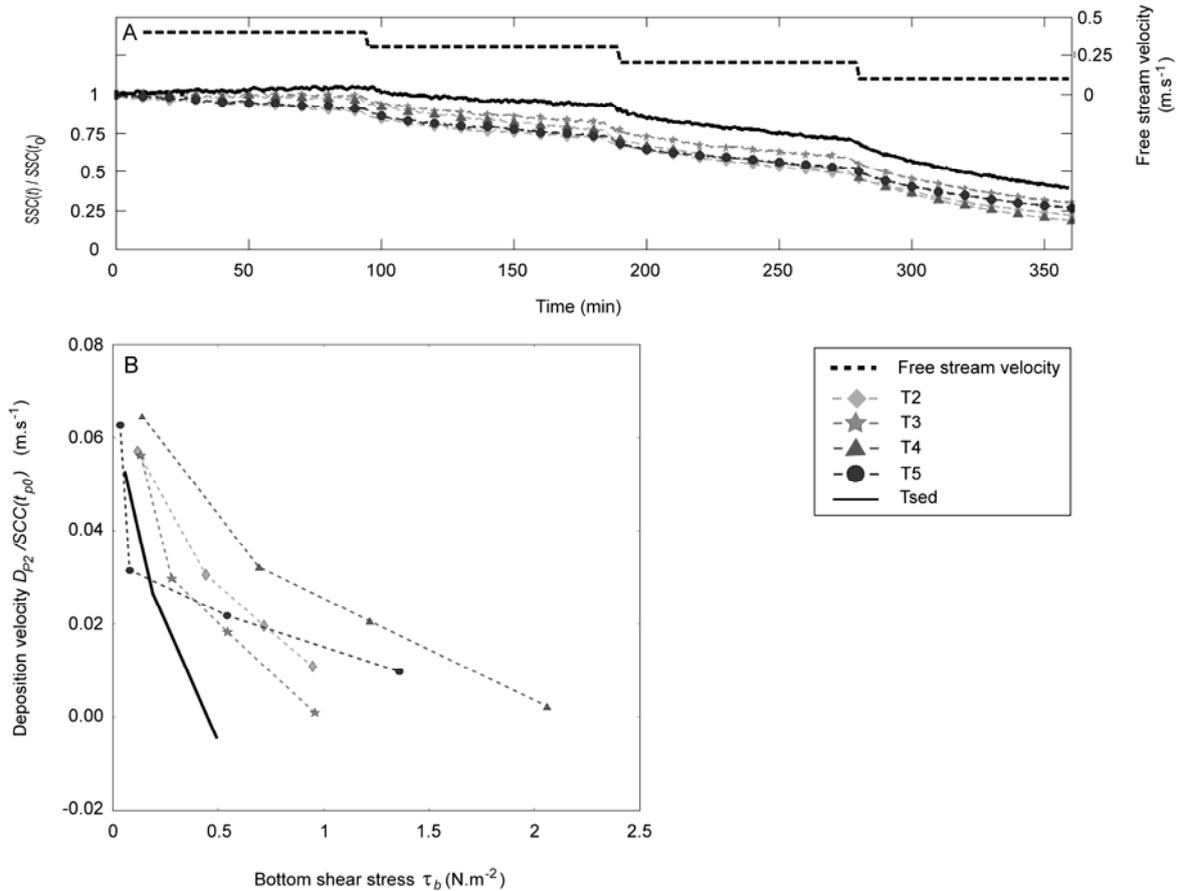
Fig. 8: (A) Time series of normalized suspended sediment concentration during the second experiment phase (P2) over different densities of *Zostera noltei* (T2 to T5, dashed lines) and the control (Tsed, solid black line). Time-series of suspended sediment concentration were normalized by suspended sediment concentration measured at t_0 (when the flume was seeded and considered homogene, see Table 2 for $SSC(t_0)$ values). Bold dashed black line corresponds to the free-stream velocity applied at each velocity step. (B) Relationship between apparent deposition velocities (deposition fluxes divided by the concentration at the beginning of each velocity step) at each velocity step and bottom shear stress above vegetated beds (T2 to T5) and bare sediments (Tsed).

Because suspended sediment concentrations at the beginning of each velocity step differed significantly, deposition fluxes (D_{P2}) were converted into apparent deposition velocities by dividing them by the suspended concentration at the beginning of each velocity step ($SSC(t_{p0})$). The deposition velocities then obtained in all tests with vegetated beds (T2 to T5, $D_{P2}/SSC(t_{p0}) = 0.001 – 0.065$ m.s^{-1}) were higher than those obtained in the control test (Tsed, $D_{P2}/SSC(t_{p0}) = -0.005 – 0.052$ m.s^{-1}, Fig. 8B). At low velocities ($U_\infty = 0.1 – 0.3$ m.s^{-1}), lower values ($0.015 – 0.063$ m.s^{-1}) were measured in the least developed seagrass bed (T2 and T3) and in the most developed (T5), while the highest values ($0.023 – 0.066$ m.s^{-1}) were measured in the seagrass bed in T4. In contrast, at the highest velocity ($U_\infty = 0.4$ m.s^{-1}), test T5 had the highest deposition velocity (0.011 m.s^{-1}), despite high bottom shear stress.

Erosion of freshly deposited sediment: Phase P3
Time series of suspended sediment concentrations (SSC, Fig. 9A) had similar step or stair shape in all tests (T2 to T5 and Tsed) during the third experimental phase (P3). The resuspension of freshly deposited sediments appeared to be higher in the most developed seagrass beds (T5). In contrast, *SSC* levels were lower in the less developed seagrass beds (T2). The concentrations measured in the control test were within the extreme levels obtained in the vegetated beds.

The relationship between erosion fluxes (E_{P3}) and bottom shear stress (τ_b) (Fig. 9B) highlighted limited resuspension in the case of low to moderate seagrass development (T2 to T4) at low velocities ($U_\infty = $

0.1 – 0.2 m.s^{-1}), compared with the control test (Tsed). In contrast, the erosion fluxes in the most developed seagrass bed (T5) were higher than those in the control test. Finally, erosion fluxes generally decreased from the third velocity step ($U_\infty = 0.3$ m.s^{-1}) to the fourth ($U_\infty = 0.4$ m.s^{-1}) in the T3 to T5 and Tsed tests.
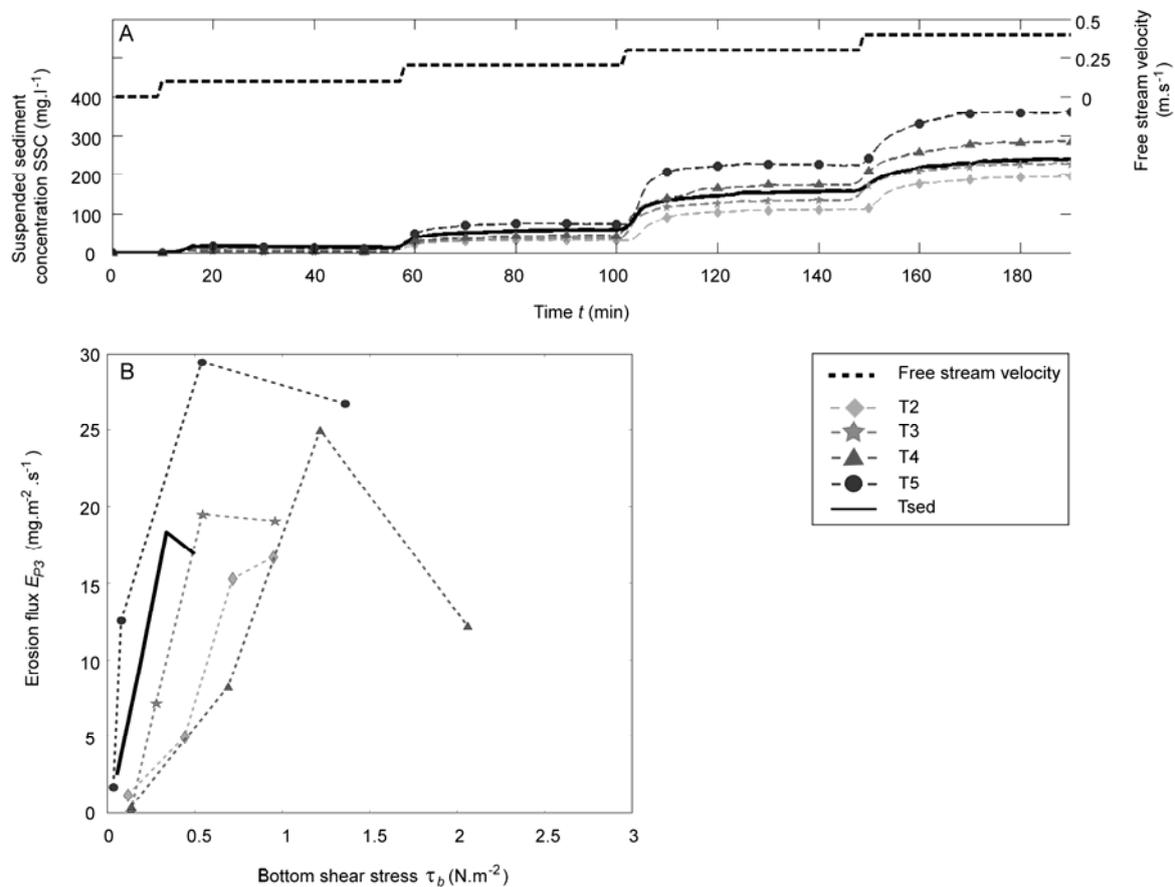

Fig. 9: (A) Time series of suspended sediment concentration during the third experimental phase (P3) over different densities of *Zostera noltei* (T2 to T5, dashed lines) and the control (Tsed, solid black line). Bold dashed black line corresponds to the free stream velocity applied at each velocity step. (B) Relationship between erosion fluxes at each velocity step and bottom shear stress above vegetated beds (T2 to T5) and a bare sediments (Tsed).

DISCUSSION

Response of *Zostera noltei* canopies to their ambient flow

As reported by many authors (e.g., Peralta et al., 2008; Widdows et al., 2008), the height of the canopy (Hc_m, measured from digital photography analysis) decreased with increasing free stream velocity (Fig. 10, Table 4) in response to increasing drag forces acting on the seagrass leaves. Deflection of the canopy reduced the canopy volume, resulting in a high-density leaf layer near the bottom. This canopy reconfiguration tended to reduce the drag forces acting on leaves, due to their more streamlined position (Koehl, 1994), so that the maximum leaf bending resulted from the balance between the drag forces and the strength of leaves (Luhar and Nepf, 2011). Porosity within the canopy was also reduced by canopy reconfiguration, so that in cases of considerably deflected canopies, at both flow velocities and vegetation densities, contact between the leaves themselves may limit bending. Thus, canopy bending is not a linear function of current velocity but included both the ambient current velocity and vegetation characteristics (i.e., leaf density, leaf length). Previous studies were undertaken to develop mathematical formulations to describe vegetation bending and associated canopy reconfiguration

(Erduran and Kutija, 2003; Abdelrhman, 2007; Luhar and Nepf, 2011). These formulations incorporate the balance between the drag forces acting on separated leaves and leaf flexibility (i.e. module of elasticity) and buoyancy. However, their use requires precise knowledge of physical parameters (module of elasticity, buoyancy) which may vary in space and time depending on the seasonal development of the seagrass. Moreover, the presence and growth of epiphytes may modify leaf roughness (with consequences for the drag forces acting on leaves). Epiphytes may also trap silty sediments leading to changes in leaf buoyancy.
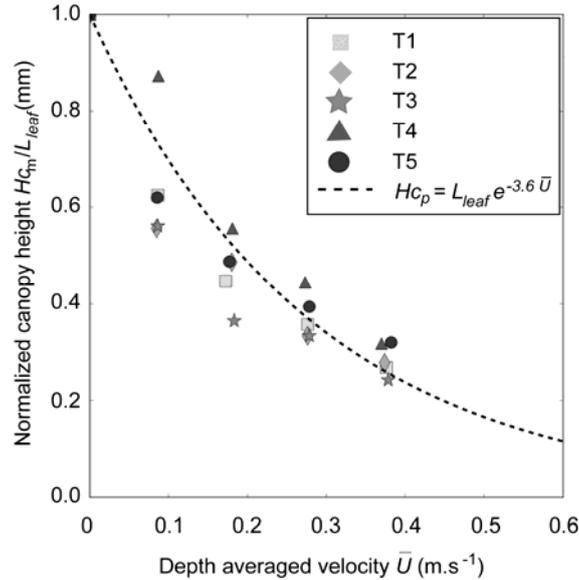

Fig. 10: Relationship between normalized canopy height (Hc_m/L_{leaf}) bent under hydrodynamics and depth averaged velocity ($\bar{U}$) for different seagrass densities (T1 to T5). Dashed line represent the exponential regression ($R^2 = 0.85$, $p<0.01$) obtained as a parameterization of the canopy height (eq. 5).

One of the aims of this study was to obtain a dataset to enable parameterization and calibration of a plant-flow interaction model to simulate the impacts of the short flexible seagrass *Z. noltei* on hydrodynamics and sediment dynamics from small scales (e.g. 1-10 m – to better understand small-scale processes) to the scale of coastal systems (e.g. 10^2-10^4 m – to investigate cascading effects of the presence of vegetation on the sediment dynamics of such systems). The leaf-by-leaf models for canopy reconfiguration did not appear to be useful for a regional-scale hydrodynamic model because of the long computation time required. We consequently searched for a simpler way to parameterize the change in canopy height caused by hydrodynamic forcing. As for zero velocity, the canopy height (H_c) should be roughly equal to the length of the unbent leaf (L_{leaf}) and the magnitude of the depth-averaged velocity is strictly positive, we found a good parameterization ($R^2 = 0.85$, $p<0.01$, and *RMSE* = 6.58 mm between measured and predicted heights; Fig. 10) of the canopy height assuming an exponential decrease in canopy height depending on the magnitude of the depth-averaged velocity (5, where Hc_p is the predicted canopy height).

$$Hc_p = L_{leaf} \cdot e^{-3.6 \cdot \bar{U}} \qquad (5)$$

It should be noted that the effect of density, which may modulate canopy height through plant/plant interaction and canopy reconfiguration was not shown to be significant at first order in this study.
Although this parameterization is empirical and thus specific to *Z. noltei* seagrass, it appeared to be suitable enough to predict changes in the height of *Z. noltei* canopies depending on both hydrodynamic forcing and seagrass growth and require less computational time.

Flow modifications by *Zostera noltei* canopy

Velocity and turbulence: sparse versus dense canopies

A significantly reduced flow velocity was measured within *Zostera noltei* canopies despite their considerably shorter leaves compared with taller species (Fonseca and Fisher, 1986; Gacia et al., 1999; Koch, 1999; Granata et al., 2001; Hendriks et al., 2008). In all cases, near-bed flows within the canopy were dramatically reduced, but nevertheless varied in response to the development stage of *Z. noltei*. Two groups were identified (Fig. 11) with opposite behaviour: from T1 to T3, increasing the depth averaged velocity was associated with a decrease in near bed velocity attenuation, while from T4 to T5, increasing the velocity yielded stronger near bed velocity attenuation. These different behaviours are caused by the competition between the bed-induced rough-wall boundary layer and the canopy-induced shear layer and their subsequent modulation by the features of the meadows (Nepf, 2012). In sparse canopies (i.e. T1 to T3), flow penetrates the entire canopy and turbulence intensities increase with frontal area. Lacy and Wyllie-Echeverria (2011) demonstrated that in sparse canopies, the bottom boundary layer is predominant compared with the vegetation-induced shear layer, which only contributes to bed roughness. This dominance increases with increasing velocity as flow can accelerate between leaves due to canopy reconfiguration (Fonseca et al., 1983; Nepf, 1999; Lawson et al., 2012). This consequently causes lower velocity attenuation with increasing velocity, as observed in the present study. In dense canopies (T4-T5), the entire flow is deflected above the canopy, which is then completely separated from the overlying flow. In that case, the mutual sheltering of individual leaves is emphasized in bent canopies (through canopy reconfiguration) and is associated with a more deflected flow above the canopy. This was observed in this study with the presence of an inflection point on velocity profiles indicating the full development of the shear layer (Fig. 3). This finally leads to greater reduction of the momentum penetration within the canopy (Luhar et al., 2008) and higher velocity attenuation with increasing velocity.
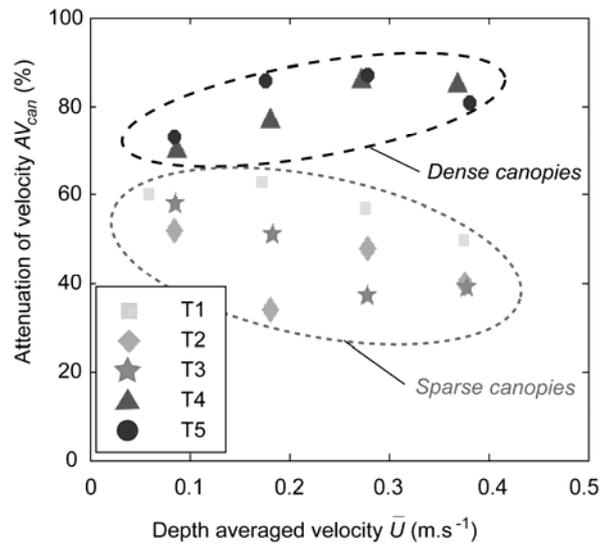

Fig. 11: Relationship between the attenuation of velocity (AV_{can}, eq. 3), inside the canopy and the depth-averaged velocity ($\overline{U}$) for different seagrass densities (T1 to T5). The two groups significantly delineated by a Turkey's test are indicated by dashed ellipsis.

Nepf (2012) described the transition from sparse and dense canopy behaviour through the non-dimensional canopy frontal area index λ_f (6):

$$\lambda_f = \int_0^{Hc_m} a \cdot dz \qquad (6)$$

where a is the frontal area per canopy volume. In this case, a was assumed to be equal to $w_{leaf}D_{leaf}$ and a uniform vertical leaf density was considered in absence of reliable data on the canopy vertical configuration. Calculating the canopy frontal index for all tests confirmed the presence of two distinct groups: in tests T1-T2-T3 (sparse canopies) λ_f was equal to 0.84, 1.43 and 1.76 respectively, while in T4 and T5, λ_f ranged from 4.18 to 9.04. The sparse/dense transition value obtained in this study ($\lambda_f \approx$ 2) is larger than values reported in the literature (λ_f ranging from 0.1 to 0.5; Luhar et al., 2008).

However, these values were obtained for *Zostera marina* meadows, and we suspect that λ_f transition value is species-dependant.

Differences between sparse and dense canopies also have major implications for turbulence production. Gambi et al. (1990) recorded a 10-fold increase in turbulence at the canopy-water interface and within the canopy of *Zostera marina*. Widdows et al. (2008) found a comparable increase in turbulence in *Z. noltei* beds. Similarly, results revealed an increase (although smaller) in the *TKE* within the canopies (compared with unvegetated bed profiles): a 4-fold increase at the water-canopy interface and a 2.5-fold increase near the bottom (Fig. 4). However, a transition in the shape of the *TKE* profiles was found depending on the seagrass density. In sparse canopies (T1 to T3), turbulence was maximum close to the bed and decreased upward. As reported for the changes observed in vertical velocity profiles in sparse canopies, the flow penetrates the entire canopy and behaves as a bottom boundary layer flow, with apparent roughness including both bed and vegetation features (Nepf et al., 2007a, 2007b; Widdows et al., 2008; Lacy and Wyllie-Echeverria, 2011). In dense canopies (T4 and T5), the maximum occurred higher in the water column just below the water-canopy interface: the development of the shear layer induced by the deflection of the flow above the canopy is an important source of turbulence, while near-bed turbulence is much reduced (Nepf and Vivoni, 2000; Luhar et al., 2008).

A linear relationship (p < 0.001, Fig. 12) between the canopy height (Hc_m) and the height of the maximum *TKE* value (called H_{TKE}), was observed, independently of seasonal growth. H_{TKE} coincided with the location of the highest mean shear (i.e. the inflection point in the velocity profiles, Fig. 3 and 4). H_{TKE} appeared roughly equal to 0.7-fold the canopy height and thus did not strictly corresponds to the water-canopy interface, as already observed in previous studies performed on both rigid and flexible plant species, but not on *Z. noltei* (Sand-Jensen and Pedersen, 1999; Neumeier and Amos, 2004; Widdows et al., 2008; Chen et al., 2011). This lower maximum turbulence zone was attributed to the extreme leaf flexibility, which led to the formation of a dense leaf layer with a lower drag because the leaves were horizontally aligned with the flow (Madsen et al., 2001; Fonseca et al., 2007).
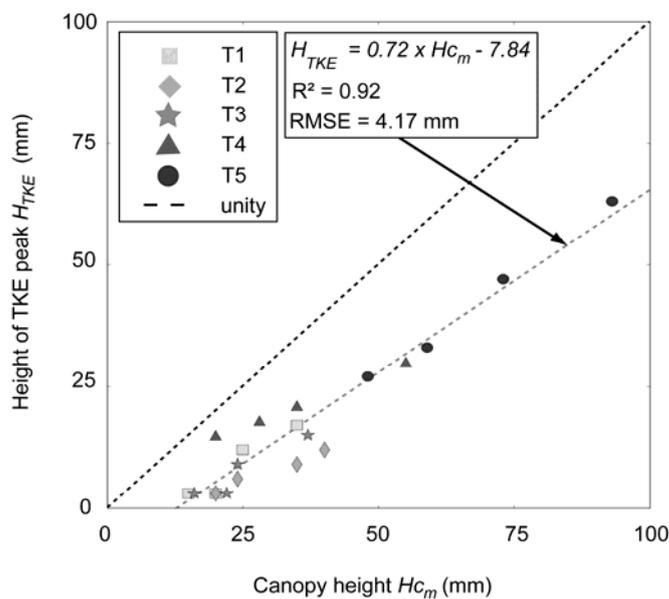

Fig. 12: Relationship between height of the maximum TKE value (H_{TKE}) and measured canopy height for the different densities of seagrass (T1 to T5). The significant linear regression (dashed grey line), its equation and the RMSE between the observed H_{TKE} and predicted H_{TKE} are given.

Relative impacts of vegetation characteristics on flow modification

The relative impacts of vegetation characteristics on flow modifications by *Z. noltei* were also statistically investigated. We searched for significant linear relationships between the reduced-centered velocity attenuation coefficient and the main variables describing the characteristics of the canopies (leaf area index, leaf density, canopy height, and submergence depth – h/Hc_m). As expected, the most significant vegetation variable explaining variation in velocity attenuation coefficient was the leaf area

index (*LAI,* R²=0.59, p<0.01), which includes all vegetation variables (leaf density, height and width). However, considering that leaf density and canopy height did not vary during seagrass development, leaf density (D_{leaf}) appeared to better describe changes in velocity attenuation than canopy height, Hc_m, (R²= 0.45, p<0.01 for leaf density, and R²=0.28, p<0.05 for canopy height), while the submergence depth was not found to be a significant parameter. This finding also confirmed the fact that, during *Z. noltei* seasonal growth, the vertical flow distribution (velocity and turbulence profiles) is predominantly driven by leaf density and associated thresholds, rather than by the increase in leaf length. The predominant effect of leaf density over canopy height could be attributed to the short stature of *Z. noltei* canopies.

Bottom shear stress

Bottom shear stress was found to be significantly enhanced in presence of seagrass, in comparison with a bare bed, except for high-density meadows associated with high canopies (test T5 at low velocities), when a slight decrease was found. Results showed that bottom shear stress increased with increasing velocity, but with no clear correlation with either seagrass density or height (Fig. 5). This is consistent with previous field and flume studies performed on *Z. noltei*, *Z. marina* and *Spartina anglica* (Gambi et al., 1990; Fonseca and Khoel, 2006; Bouma et al., 2007; Widdows et al., 2008; Lefebvre et al., 2010). These authors reported an increase in bottom shear stress with increasing distance from the leading edge of the vegetation patch in relation to the flow deceleration and turbulence production caused by friction on the bed and on vegetation stems (Gambi et al., 1990; Lefebvre et al., 2010). Using flume and field experiments and numerical modelling, Bouma et al. (2007) showed that upon entering a patch of vegetation, bottom shear stress first increases until the flow within and above the canopy is fully developed. Afterwards, turbulence and hence bottom shear stress, decrease. The distance currents can penetrate the edge of a seagrass bed before becoming equilibrated with respect to momentum has been estimated to range between 1 m (Fonseca and Fisher, 1986) and 50 boundary layers (assumed to be equal to the height of the canopy; Nowell and Jumars, 1984; Granata et al., 2001). In this study, we would estimate this distance to range from 0.75 to 4.65 m, so that measurements performed at 0.45 m from the leading edge of the patch may still be representative of the patch-edge transition zone. However, these values can questioned as they may depend on the type and density of the vegetation as well as on the vertical distribution of biomass (Koch and Gust, 1999; Van Keulen et al., 2003).
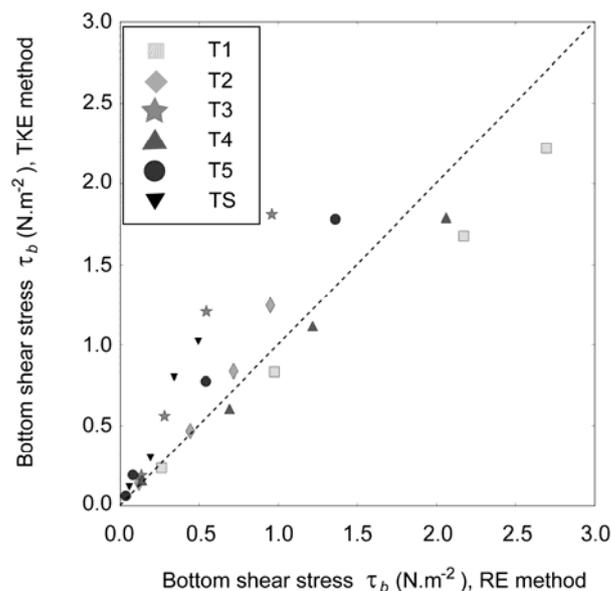

Fig. 13: Comparison between bottom shear stress (τ_b) computed following the Reynolds stress method (RE) and the turbulent kinetic energy method (TKE). Dashed line represents the unity line.

Direct comparison of the two methods used to compute the bottom shear stress (Fig. 13) showed that results obtained with the TKE method were in the same order of magnitude as those obtained using the RE method (RMSE = 0.32 N.m^{-2}). However, some discrepancies were found. For tests T1 and T4, the TKE method tended to underestimate bottom shear stress compared with the RE method. On the contrary, for tests T2, T3, T5 and Tsed, the TKE methods led to overestimation of the bottom shear stress. Different values for the empirical coefficient ($C1$) were found depending on tests. The values ranged from 0.09 to 0.24 (respectively for test Tsed and T1), but without any clear trends depending on vegetation characteristics. Using the TKE method with the standard C1 value (0.19) did not appear to modify the main trends over all tests (i.e. bare mud versus vegetated test).

Implications of flow modification by seagrass for sediment erosion and deposition processes

The seasonal development of *Zostera noltei* meadows associated with their high flexibility strongly influenced velocity, turbulence, and bottom shear stress, and subsequent erosion/deposition processes within the meadow. These effects on sediment processes were investigated through the quantification of erosion and deposition fluxes. The device used to assess sediment fluxes (a single turbidity probe) means that the temporal variability of bedload transport and the vertical distribution of *SSC* could not be captured in this study. However, due to the high turbulence levels associated with small grain sizes, sediments were likely transported in suspension and differences in vertical *SSC* gradients are assumed to remain limited. The negligibility of the bedload transport was confirmed by the absence of significant amounts of sediments collected in a sand trap located downstream from box cores during all the tests, while the ability of the sand-trap to effectively trap sediments was confirmed during a preliminary test performed with only pure medium sand. The main limitation for a detailed investigation of sediment processes could be the absence of information about the spatial (i.e. longitudinal) pattern of sediment transport processes along patches of seagrass of limited (O(m)) length. In this study, sediment erosion-deposition fluxes can be safely considered as representative of the general erosion-deposition patterns occurring over the whole seagrass patches, while spatial differences in sediment erosion-deposition from the edges to the middle of the seagrass patch could be captured.

Nonetheless, the use of seagrasses sampled with their sediments beds enabled assessment of resuspension of sediments presenting the same erosion behaviour as those found in the field (i.e. sediment composition, consolidation stage, or biological effects such as root binding).

Although seagrass beds are generally believed to stabilise bed sediments (Fonseca and Fisher, 1986; Gacia et al., 1999; Bos et al., 2007), erosion fluxes confirm that sediment resuspension can occur due to near-bed turbulence within canopies, even at low velocities. However, this study confirmed that *Z. noltei* canopies enhanced net (at the tidal scale) sediment deposition, despite the occurrence of higher bottom shear stresses compared with the unvegetated bed, i.e. a positive budget between deposition and resuspension.

During the first experimental phase (P1) and in sparse canopies (i.e., tests T1, T2 and T3) the erosion fluxes (Fig. 14A) appeared mostly controlled by the physical properties of sediment beds including a decrease in dry density and an increase in mud content, which are known to affect sediment erodibility (Mitchener and Torfs, 1996; Aberle, 2004; Ganthy et al., 2011; Jacobs et al., 2011). Many studies demonstrated that these changes in bed sediment properties depending on seagrass density are the consequence of the seasonal development of the seagrass meadows throughout their growth (Heiss et al., 2000; Bos et al., 2007; van Katwijk et al., 2010; Ganthy et al., 2013). However, in dense canopies (tests T4 and T5) with comparable sediment characteristics (i.e., comparable erodibility behaviour), the bed was found to be more protected from erosion by seagrass beds with a taller canopy and a higher *LAI* (test T5), despite a lower leaf density compared to test T4 (Fig. 14A). This result could be related to the higher position of the maximum turbulence intensity in test T5 than in test T4, which tended to decrease near-bed turbulence and thus helped protect the bed from erosion at both high and low current velocities (Ward et al., 1984; Peralta et al., 2008; Widdows et al., 2008). Furthermore, in tests with low canopy heights (tests T1 to T4) and at high velocities ($U_\infty = 0.3$ and 0.4 m.s^{-1}) we observed that seagrass leaves flapped and hit the bed. This process may destabilize the deb sediments and may explain the higher erosion fluxes measured in test T4 than in test T5, despite the similar sediment characteristics.
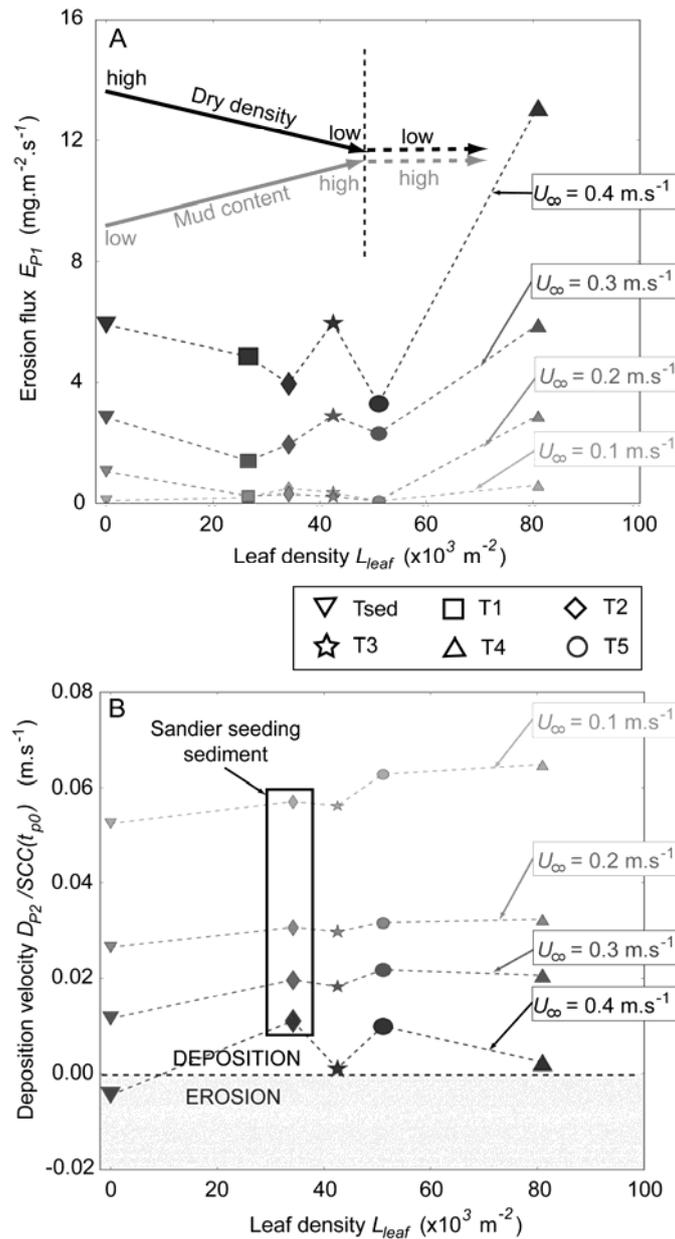
Fig. 14: (A) Relationship between erosion fluxes (E_{P1}) measured during the first experimental phase (P1) and leaf density (D_{leaf}) for different densities of seagrass (T1 to T5, different markers) and control (Tsed), as a function of applied free stream velocities (U_∞, different colours and marker sizes). General trends for dry density and mud content measured before experiments (Table 2) are also presented. (B) Relationship between deposition velocities (deposition fluxes, D_{P2}, divided by the concentration at the beginning of each velocity step, $SSC(t_{p0})$) measured during the second experimental phase (P2) and leaf density (D_{leaf}) for different densities of seagrass (T1 to T5, different markers) and control (Tsed), as a function of applied free stream velocities (U_∞, different colours and marker sizes).

Although Gacia and Duarte (2001) conclude that seagrass meadows often reduce resuspension rather than enhance deposition, erosion fluxes measured during the second experimental phase (P2) indicated that *Z. noltei* meadows are able to significantly enhance deposition. Deposition velocities ($D_{P2}/SSC(t_{p0})$) tended to increase with an increase in leaf density at low to moderate velocities (Fig. 14B), when less leaf bending occurred, resulting in an "open" canopy. In this case, most of the suspended particles transported within the canopy are likely to collide with the leaves, leading to their capture by loss of momentum (Ackerman, 2002; Hendriks et al., 2008). Also, the probability of a

particle hitting a leaf increased with the leaf density. In contrast, at a high flow velocity ($U_\infty = 0.4$ m.s^{-1}), despite its lower leaf density, the tallest canopy (in test T5) was more efficient at trapping particles than test T4. These results could be related to the larger flux of water, and hence suspended sediments, passing through the taller canopy (Peralta et al., 2008). In agreement with previous studies, sediment trapping efficiency was found to be lower in short canopies than in taller canopies (Heiss et al., 2000; Mellors et al., 2002; Peralta et al., 2008). Moreover, this process could be enhanced by the presence of the shear layer induced by the high leaf density and canopy height (Nepf, 1999). In the case of submerged dense canopies, the drag discontinuity at the top of the canopy produces coherent vortices through Kelvin-Helmotz instabilities (Brown and Roshko, 1974; Ikeda and Kanazawa, 1996; Ghisalberti and Nepf, 2002, 2006) and may favour deposition.

Although the deposition fluxes were significantly higher in presence of *Z. noltei*, the results obtained during the third experimental phase (P3) showed that erosion fluxes of freshly deposited sediments (E_{P3}) tended to increase with the *LAI* (Fig. 15). This could be explained by the fact that during the deposition phase (P2), the decrease in *SSC* cannot be only related to sediment deposition onto the bed. Indeed, at the end of the deposition phase, a significant deposition of sediment on the leaves was observed. These fresh sediment deposits were then easily resuspended from the leaves when velocity was increased during the third experimental phase. Furthermore, the higher erosion fluxes (E_{P3}) obtained in test T5 compared with the unvegetated test (Tsed), may indicate that most of the sediment was deposited on leaves, while few sediments reached the bed and were protected against subsequent erosion.
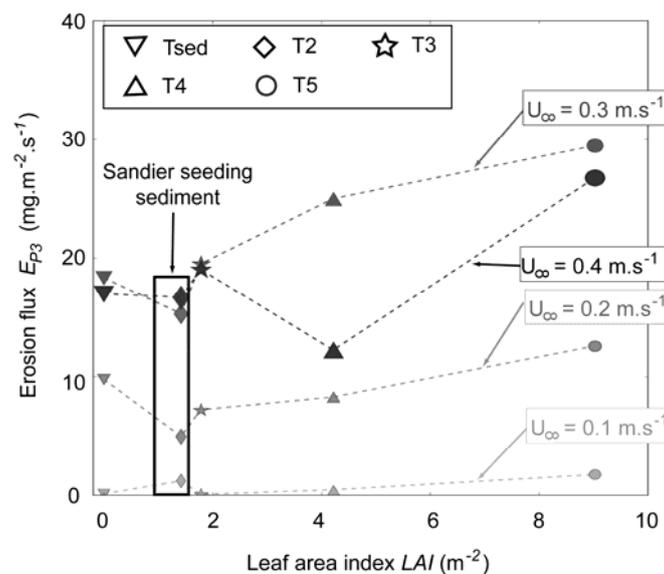

Fig. 15: Relationship between erosion fluxes (E_{P3}) measured during the third experimental phase (P3) and leaf area index (*LAI*) for different densities of seagrass (T1 to T5, different markers) and control (Tsed) depending on applied free stream velocities (U_∞, different colours and marker sizes).

Implications for sediment dynamics on a seasonal scale

The influence of *Zostera noltei* on near-bed hydrodynamics, sediment resuspension and deposition varied with the season, due to leaf growth and increased plant densities in the spring-summer period and their subsequent degeneration in autumn-winter (see Auby and Labourg, 1996). The present study was conducted from March to September, the representative period of contrasting above-ground seagrass biomass and densities. Experimental results showed that 1) erosion was higher in bare mud beds than in vegetated beds and 2) that canopy development (i.e. an increase in both density and height) increased protection against erosion. In the case of low to moderate development of seagrass, the efficiency of sediment deposition was found to be positively density-dependent. In periods of significant inputs of suspended sediments, results suggest that significant deposition and subsequent

accretion occur during the seagrass growth period. Assuming that velocities are equally distributed over a tidal cycle, a simple calculation can be made from erosion and deposition fluxes. In that case, net fluxes are significantly in favour of net deposition, and positively correlated with *Z. noltei* densities. These results are in agreement with *in situ* observations made during one annual cycle in the intertidal mudflat where box cores were collected in the Arcachon Lagoon by Ganthy et al. (2013): large accretion during the growing stage (accretion ranged from +15 to +41 mm in 8 months, depending on meadow coverage). When the meadow was fully developed, the accretion rate was strongly reduced; which would confirm the predominance of sediment deposition on leaves (resuspended during the next tidal cycle) as observed in these flume experiments.

CONCLUSION

Innovative erosion-deposition flume experiments were conducted in a recirculating straight flume using boxes of *Zostera noltei* meadows in their natural bed sediments sampled at contrasting stages of their seasonal growth from winter to late summer (March to September in the north Atlantic Arcachon lagoon). These experiments helped quantify the impact of seagrass development and canopy flexibility on hydrodynamics, sediment accretion and the bed stability of intertidal areas. Results also identified threshold effects related to the seasonal development stage of the plant.

Z. noltei canopies responded to their ambient flow by an exponential decrease in canopy height when the free-stream velocity increased, due to the canopy rearrangement in a near-bed dense layer of leaves, which in turn modified the flow within and above canopies. The highest vegetation densities were found to be the most efficient at increasing flow attenuation close to the bed (up to 90% attenuation), and a high flow velocity resulted in higher attenuation. Bottom shear stress was significantly enhanced by the presence of vegetation. The presence of the skimming flow at a greater distance above the bed significantly increased the bed protection against erosion. The efficiency of sediment trapping by seagrass canopies was found to be density-dependent, and hence seasonally variable, with highest net trapping at high density values. However, with a very high leaf area index, deposition occurred mostly on leaves, resulting in easier resuspension and less efficient sediment deposition on the bed than at a lower leaf density. These results are consistent with *in situ* observations made during an annual field survey conducted on the same tidal flat colonized by *Z. noltei* meadows, indicating that the small-scale processes and their seasonal variability identified in this study control colonized tidal flats at larger temporal and spatial scales.

These experimental results provide a valuable dataset that will be used to modify hydrodynamics and sediment transport formulation in presence of vegetation in 3D numerical models. These models will enable the investigation of spatial heterogeneities such as meadow patchiness at the meadow scale and the influence of meadows on the dynamics of the coastal systems.

ACKNOWLEDGEMENTS

NOMENCLATURE

a	frontal area per canopy volume
AV_{can}	velocity attenuation coefficient within vegetation canopy
B_{above}	aboveground biomass

C_{mud}	mud content of sediments
$C1$	constant for bottom shear computation from the turbulent kinetic energy
D_{10}, D_{50}, D_{90}	sediment grain size for 10th, 50th, and 90th percentiles
D, D_{P2}	deposition flux and deposition fluxes for experimental phase P2, respectively
D_{leaf}	leaf density
D_{shoot}	shoot density
E, E_{P1}, E_{P3}	erosion flux and erosion fluxes for experimental phases P1 and P3, respectively
h	water depth
Hc_m	measured canopy height
H_{TKE}	height of the maximum turbulent kinetic energy
LAI	leaf area index
L_{leaf}	leaf length
M_{dry}	dry sediments mass
$M_{e/d}(t)$	instantaneous eroded or deposited sediment mass
M_{fresh}	fresh sediment mass
M_p	mass of empty ill-box
$Mseed_{dry}$	dry mass of seeded sediments
$Mseed_{fresh}$	fresh mass of seeded sediments
N	turbidity
$RMSE$	root mean square error
S_l	water salinity
S	active surface area for erosion or deposition
S_{P1}, S_{P3}	active surface area for erosion during experimental phases P1 and P3, respectively
S_{P2}	active surface area for deposition during experimental phase P2
SSC, a_{SSC}, b_{SSC}	suspended sediment concentration, and calibration coefficients for suspended sediment concentration, respectively
T	water temperature
t	time
t_0	seedling time
tp_0	time of velocity change
TKE	turbulent kinetic energy
u', v', w'	turbulent velocity components
U, V, W	time-averaged velocity components in downstream, cross-stream and vertical directions, respectively
$U(z)$	velocity at height z
$U_s(z)$	velocity at height z for control test without vegetation
$U_v(z)$	velocity at height z for vegetated test
$\overline{U}$	depth-averaged velocity
U_∞	free stream velocity
u^*	friction velocity
V_f	water volume of the flume
V_t	total volume of pill-box
w_{leaf}	mean leaf width
$W_\%$	water content of sediments
x, y, z	positions in downstream, cross-stream and vertical directions, respectively
z_0	bed roughness length
κ	von Kamran constant
λ_f	non-dimensional canopy frontal area index
ρ	water density
ρ_{dry}	dry density of sediments
τ_b	bottom shear stress

REFERENCES

Abdelrhman, M.A. (2007). Modeling coupling between eelgrass *Zostera marina* and water flow. *Mar. Ecol. Prog. Ser.*, 338, 81-96.

Aberle, J. (2004). Effects of bed material properties on cohesive sediment erosion. *Mar. Geol.*, 207, 83-93.

Ackerman, J.D. (2002). Diffusivity in a marine macrophyte canopy: implications for submarine pollination and dispersal. *Aquat. Bot.*, 89, 1119-1127.

Amos, C.L., Bergamasco, A., Umgiesser, G., Cappucci, S., Cloutier, D., DeNat, L., Flindt, M., Bonardi, M. and **Cristante, S.** (2004). The stability of tidal flats in Venice Lagoon - the results of in-situ measurements using two benthic, annular flumes. *Journal of Marine Systems*, 51, 211-241.

Amos, C.L., Umgiesser, G., Ferrarin, C., Thompson, C.E.L., Whitehouse, R.J.S., Sutherland, T.F. and **Bergamasco, A.** (2010). The erosion rates of cohesive sediments in Venice lagoon, Italy. *Cont. Shelf Res.*, 30, 859-870.

Auby, I. and **Labourg, J.-P.** (1996). Seasonal dynamics of *Zostera noltii* Hornem. in the bay of Arcachon (France). *Journal of Sea Research*, 34, 269-277.

Auby, I., Oger-Jeanneret, H., Sauriau, P.-G., Hily, C. and **Barillé, L.** (2010). Angiospermes des côtes françaises Manche-Atlantique. Proposition pour un indicateur DCE et première estimation de la qualité. Ifremer Technical Report RST/LER¨MPL/10-15, Brest (France). online document in French. http://archimer.ifremer.fr/doc/00032/14358/11646.pdf.

Biron, P.M., Robson, C., Lapointe, M. and **Gaskin, S.J.** (2004). Comparing different methods of bed shear stress estimates in simple and complex flow fields. *Earth Surf. Process. Landforms*, 29, 1403-1415.

Bos, A.R., Bouma, T.J., de Kort, G.L.J. and **van Katwijk, M.M.** (2007). Ecosystem engineering by annual intertidal seagrass beds: sediment accretion and modification. *Estuar. Coast. Shelf. Sci.*, 74, 344-348.

Bouma, T.J., De Vries, M.B., Low, E., Peralta, G., Tànczos, I.C., Van De Koppel, J. and **Herman, P.M.J.** (2005). Trade-offs related to ecosystem engineering: a case study on stiffness of emerging macrophytes. *Ecology*, 86, 2187-2199.

Bouma, T.J., van Duren, L.A., Temmerman, S., Claverie, T., Blanco-Garcia, A., Ysebaert, T. and **Herman, P.M.J.** (2007). Spatial flow and sedimentation patterns within patches of epibenthic structures: combining field, flume and modelling experiments. *Cont. Shelf. Res.*, 27, 1020-1045.

Brown, G.L. and **Roshko, A.** (1974). On density effects and large structure in turbulent mixing layers. *J. Fluid Mech.*, 64, 775-816.

Cea, L., Puertas, J. and **Pena, L.** (2007). Velocity measurements on highly turbulent free surface flow using ADV. *Exp. Fluids* 42, 333-348.

Chanson, H., Trevethan, M. and **Aoki, S.** (2008). Acoustic Doppler velocimetry (ADV) in small estuary: field experience and signal post-processing. *Flow Measurement and Instrumentation*, 19 (5), 307-313.

Chen, S., Sanford, L.P., Koch, E.W., Shi, F., and **North, E.W.** (2007). A nearshore model to investigate the effects of seagrass bed geometry on wave attenuation and suspended sediment transport. *Est. Coasts*, 30(2), 296-310.

Chen, S.C., Kuo, Y.M. and **Li, Y.H.** (2011). Flow characteristics within different configurations of submerged flexible vegetation. *J. Hydrol.*, 298, 124-134.

De Langre, E., (2008). The effects of wind on plants: a review. *Ann. Rev. Fluid Mech.*, 40, 141-168.

Deloffre, J., Verney, R., Lafite, R., Lesueur, P., Lesourd, S. and **Cundy, A.B.** (2007). Sedimentation on intertidal mudflats in the lower part of macrotidal estuaries: sedimentation rhythms and their preservation. *Mar. Geol.*, 241 (1-4), 19-32.

Erduran, K.S. and Kutija, V. (2003). Quasi-three-dimensional numerical model for flow through flexible, rigid, submerged and non-submerged vegetation. *J. Hydroinformatics*, 05 (3), 189-202.

Fonseca, M.S. and **Fisher, J.S.** (1986). A comparison of canopy friction and sediment movement between four species of seagrass with reference to their ecology and restoration. *Mar. Ecol. Prog. Ser.*, 29, 15-22.

Fonseca, M.S. and **Koehl, M.A.R.** (2006). Flow in seagrass canopies: the influence of patch width. *Estuar. Coast. Shelf. Sci.*, 67, 1-9.

Fonseca, M.S., Koehl, M.A.R. and **Kopp, B.S.** (2007). Biomechanical factors contributing to self-organization in seagrass lanscapes. *J. Exp. Mar. Biol. Ecol.*, 340, 227-246.

Fonseca, M.S., Zieman, J.S., Thayer G.W. and **Fisher, J.S.** (1983). The role of current velocity in structuring eelgrass (*Zostera marina* L.) meadows. *Estuar. Coast. Shelf. Sci.* ,17, 367-380.

Gacia, E. and **Duarte, C.M.** (2001). Sediment retention by a Mediterranean *Posidonia oceanica* meadow: the balance between deposition and resuspension. *Estuar. Coast. Shelf. Sci.*, 52, 505-514.

Gacia, E., Duarte, C.M., Marbà, N., Terrados, J., Kennedy, H., Fortes, M.D. and **Tri, N.H.** (2003). Sediment deposition and production in SE-Asia seagrass meadows. *Estuar. Coast. Shelf. Sci.*, 56, 909-919.

Gacia, E., Granata, T.C. and **Duarte, C.M.** (1999). An approach to measurement of particle flux and sediment retention within seagrass (*Posidonia oceanica*) meadows. *Aquat. Bot.*, 65, 255-268.

Gambi, M.C., Nowell, A.R.M. and **Jumars, P.A.** (1990). Flume observations on flow dynamics in *Zostera marina* (eelgrass) beds. *Mar. Ecol. Prog. Ser.*, 61, 159-169.

Ganthy, F., Sottolichio, A. and **Verney, R.** (2011). The stability of vegetated tidal flats in a coastal lagoon through quasi in-situ measurements of sediment erodibility. *J. Coastal Res.*, SI 64, 1500-1504.

Ganthy, F., Sottolichio, A. and **Verney, R.** (2013). Seasonal modification of tidal flat sediment dynamics by seagrass meadows of *Zostera noltii* (Bassin d'Arcachon, France). *J. Mar. Sys.*, 109-110, S233-S240.

Ghisalberti, M. and **Nepf, H.M.** (2002). Mixing layer and coherent structures in vegetated aquatic flows. *J. Geophys. Res.*, 3, 1-11.

Ghisalberti, M. and **Nepf, H.M.** (2006). The structure of the shear layer in flows over rigid and flexible canopies. *Environ. Fluid Mech.*, 6, 277-301.

Granata, T.C., Serra, T., Colomer, J., Casamitjana, X., Duarte, C.M. and **Gacia, E.** (2001). Flow and particle distribution in a nearshore seagrass meadow before and after a storm. *Mar. Ecol. Prog. Ser.*, 218, 95-106.

Hansen, J.C.R. and **Reidenbach, M.A.** (2013). Seasonal growth and senescence of a *Zostera marina* seagrass meadow alters wave-dominated flow and sediment suspension within a coastal bay. *Estuar. Coast. Shelf Sci.*, 36, 1099-1114.

Hasegawa, N., Hori, M. and **Mukai, H.** (2008). Seasonal changes in eelgrass functions: current velocity reduction, prevention of sediment resuspension, and control of sediment-water column nutrient flux in relation to eelgrass dynamics. *Hydrobiologia*, 596, 387-399.

Heiss, W.M., Smith, A.M. and **Probert, P.K.** (2000). Influence of the small intertidal seagrass *Zostera novazelandica* on linear water flow and sediment texture. *NZ J. Mar. Fresh. Res.*, 34, 689-694.

Hendriks, I.E., Bouma, T.J., Morris, E.P. and **Duarte, C.M.** (2010). Effects of seagrasses and algae of the *Caulerpa* family on hydrodynamics and particle-trapping rates. *Marine Biology*, 157, 473-481.

Hendriks, I.E., Sintes, T., Bouma, T.J. and **Duarte, C.M.** (2008). Experimental assessment and modeling evaluation of the effects of the seagrass *Posidonia oceanica* on flow and particle trapping. *Mar. Ecol. Prog. Ser.*, 356, 163-173.

Ikeda, S. and **Kanazawa, M.** (1996). Three-dimensional organized vortices above flexible water plants. *J. Hydraul. Eng.*, 122, 634-640.

Jacobs, W., Le Hir, P., Van Kesteren, W. and **Cann, P.** (2011). Erosion threshold of sand-mud mixtures. *Cont. Shelf Res.*, 31, S14-S25.

Kim, S.-C., Friedrichs, C.T., Maa, J.P.-Y. and **Wright, L.D.** (2000). Estimating bottom shear stress in tidal boundary layer from acoustic Doppler velocimeter data. *J. Hydraulic Eng.*, 126, 399-406.

Koch, E.W. 1999. Sediment resuspension in a shallow *Thalassia testudinum* banks ex König bed. *Aquat. Bot.*, 65, 269-280.

Koch, E.W. and **Gust, G.** (1999). Water flow in tide- and wave-dominated beds of the seagrass *Thalassia testudinum. Mar. Ecol. Prog. Ser.*, 184, 63-72.

Koehl, M.A.R. (1984). How do the benthic organisms withstand moving water. *Am. Zool.*, 24, 57-70.

Lacy, J.R. and **Wyllie-Echeverria, S.** (2011). The influence of current speed and vegetation density on flow structure in two macrotidal eelgrass canopies. *Limnol. Oceanogr.*, 1, 38-55.

Lawson, S.E., McGlathery, K.J. and **Wiberg, P.L.** (2012). Enhancement of sediment suspension and nutrient flux by benthic macrophytes at low biomass. Mar. *Ecol. Prog. Ser.*, 448, 259-270.

Lefebvre, A., Thompson, C.E.L. and **Amos, C.L.** (2010). Influence of *Zostera marina* canopies on unidirectional flow, hydraulic roughness and sediment movement. *Cont. Shelf Res.*, 30, 1783-1794.

Leonard, L.A. and **Croft, A.L.** (2006). The effect of standing biomass on flow velocity and turbulence in Spartina alterniflora canopies. *Estuar. Coast. Shelf. Sci.*, 69, 325-336.

Luhar, M., and **Nepf, H.** (2011). Flow-induced reconfiguration of buoyant and flexible aquatic vegetation. *Limnol. Oceanogr.,* 56(6), 2003-2017.

Luhar, M., Rominger, J. and **Nepf, H.** (2008). Interaction between flow, transport and vegetation spatial structure. *Environ. Fluid Mech.*, 8, 423-439.

Madsen, J.D., Chambers, P.A., James, W.F., Koch, E.W. and **Westlake, D.F.** (2001). The interaction between water movement, sediment dynamics and submersed macrophytes. *Hydrobiologia*, 444, 71-84.

Mellors, J., Marsh, T., Carruthers, T.J.B. and **Waycott, M.** (2002). Testing the sediment-trapping paradigm of seagrass: do seagrasses influence nutrient status and sediment structure in tropical intertidal environments. *Bull. Mar. Sci.*, 71, 1215-1226.

Mitchener, H. and **Torfs, H.** (1996). Erosion of mud/sand mixtures. *Coast. Eng.* 29, 1-25.

Nepf, H.M. (1999). Vertical secondary flows in submersed plant-like arrays. *Limnol. Oceanogr.*, 44, 1072-1080.

Nepf, H.M. (2012). Flow and transport in region with aquatic vegetation. *Annu. Rev. Fluid Mech.*, 44, 123-142.

Nepf, H.M., Ghisalberti, M., White, B. and **Murphy, E.** (2007a). Retention time and dispersion associated with submerged aquatic canopies. *Water Resour. Res.*, 43, W04422.

Nepf, H.M. and **Vivoni, E.R.** (2000). Flow structure in depth-limited, vegetated flow. *J. Geophys. Res.*, 105, 28,547-528,557.

Nepf, H.M., White, B., Ligthbody, A. and **Ghisalberti, M.** (2007b). Transport in aquatic canopies. In: *Flow and Transport Processes with Complex Obstructions* (Eds. Y.A. Gayev, J.C.R. Hunt), *NATO Science Series*, 236, pp. 221-250. Springer, the Netherlands.

Neumeier, U. (2005). Quantification of vertical density variations of salt-marsh vegetation. *Estuar. Coast. Shelf. Sci.*, 63, 489-496.

Neumeier, U. (2007). Velocity and turbulence variations at the edge of saltmarshes. *Cont. Shelf Res.*, 27, 1046-1059.

Neumeier, U. and **Amos, C.L.** (2004). Turbulence reduction by the canopy of coastal *Spartina* salt-marshes. *J. Coastal Res.*, SI 39, 433-439.

Neumeier, U. and **Ciavola, P.** (2004). Flow resistance and associated sedimentary processes in a Spartina maritime salt-marsh. *J. Coastal Res.*, 20(2), 435-447.

Nowell, A.R.M. and Jumars, P.A (1984). Flow environments of aquatic benthos. *Annu. Rev. Ecol. Systematics*, 15, 303-328.

Orvain, F., Le Hir, P. and **Sauriau, P.-G.** (2003). A model of fluff layer erosion and subsequent bed erosion in the presence of the bioturbator, *Hydrobia ulvae. J. Mar. Res.*, 61, 823-851.

Paul, M. and **Amos, C.L.** (2011). Spatial and seasonal variation in wave attenuation over *Zostera noltii. J. Geophys. Res.*, 116, C08019.

Peralta, G., van Duren, L.A., Morris, E.P. and **Bouma, T.J.** (2008). Consequences of shoot density and stiffness for ecosystem engineering by benthic macrophytes in flow dominated areas: a hydrodynamic flume study. *Mar. Ecol. Prog. Ser.*, 368, 103-115.

Peterson, C.H., Luettich, J.R.A., Micheli, F. and **Skilleter, G.A.** (2004). Attenuation of water flow inside seagrass canopies of differing structure. *Mar. Ecol. Prog. Ser.*, 268, 81-92.

Rohlf, F.J. and **Sokal, R.R.** (1981). Statistical tables, 2nd ed. Freeman: San Francisco. 219 p.

Sand-Jensen, K. and **Pedersen, O.** (1999). Velocity gradient and turbulence around macrophyte stands in streams. *Freshwat. Biol.*, 45, 315-328.

Sokal, R.R. and **Rohlf, F.J.** (1995). Biometry: the principles and practice of statistics in biological research, 3rd ed. Freeman: New York, 859 p.

Stapleton, K.R. and **Huntley, D.** (1995). Seabed stress determination using inertial dissipation method and turbulent kinetic energy method. *Earth Surf. Proc. Land.*, 20, 807-815.

van der Heide, T., van Nes, E.H., Geerling, G.W., Smolders, A.J.P., Bouma, T.J. and **van Katwijk, M.M.** (2007). Positive feedbacks in seagrass ecosystems: implications for success in conservation and restoration. *Ecosystems*, 10, 1311-1322.

van Katwijk, M.M., Bos, A.R., Hermus, D.C.R. and **Suykerbuyk, W.** (2010). Sediment modification by seagrass beds: muddification and sandification induced by plant cover and environmental conditions. *Estuar. Coast. Shelf. Sci.*, 89, 175-181.

van Keulen, M., Paling, I.E. and **Walker, C.J.** (2003). Effect of planting unit size and sediment stabilization on seagrass transplants in Western Australia. *Restor. Ecol.*, 11(1), 50-55.

Verduin, J.J. and **Backhaus, J.O.** (2000). Dynamics of plant-flow interactions for the seagrass *Amphibolis antartica*: field observations and model simulations. *Estuar. Coast. Shelf. Sci.*, 50, 185-204.

Ward, L.G., Kemp, W.M. and **Boynton, W.R.** (1984). The influence of waves and seagrass communities on suspended particulates in estuarine embayment. *Mar. Geol.*, 59, 85-103.

Widdows, J., Pope, N.D., Brinsley, M.D., Asmus, H. and **Asmus, R.M.** (2008). Effects of seagrass beds (*Zostera noltii* and *Z. marina*) on near-bed hydrodynamics and sediment resuspension. *Mar. Ecol. Prog. Ser.*, 358, 125-126.